Spatiotemporal analysis of glioma heterogeneity reveals Col1A1 as an actionable target to disrupt tumor mesenchymal differentiation, invasion and malignancy

Andrea Comba[1,2,3], Sebastien Motsch[4], Patrick J. Dunn[1,2,3], Todd C. Hollon[1], Anna E. Argento[1,2], Daniel B. Zamler[1,2,3], Phillip E. Kish[1,5], Alon Kahana[5], Celina G. Kleer[3,6], Maria G Castro[1,2,3], Pedro R. Lowenstein[1,2,3,*]

[1]Dept. of Neurosurgery, University of Michigan Medical School, Ann Arbor, 48109, MI, USA
[2]Dept. of Cell and Developmental Biology, University of Michigan Medical School, Ann Arbor, 48109 MI, USA
[3]Rogel Cancer Center, University of Michigan medical School, Ann Arbor, 48109, MI, USA
[4]School of Mathematical and Statistical Sciences, Arizona State University, Tempe, AZ, USA
[5]Ophthalmology & Visual Science, University of Michigan Medical School, Ann Arbor, 48109 MI, USA
[6]Dept. of Pathology, University of Michigan Medical School, Ann Arbor, MI 48109, USA
*Correspondence to: pedrol@umich.edu

ABSTRACT

Intra-tumoral heterogeneity and diffuse infiltration are hallmarks of glioblastoma that challenge treatment efficacy. However, the mechanisms that set up both tumor heterogeneity and invasion remain poorly understood. Herein, we present a comprehensive spatiotemporal study that aligns distinctive intra-tumoral histopathological structures, oncostreams, with dynamic properties and a unique, actionable, spatial transcriptomic signature. Oncostreams are dynamic multicellular fascicles of spindle-like and aligned cells with mesenchymal properties. Their density correlates with tumor aggressiveness in genetically engineered mouse glioma models, and high grade human gliomas. Oncostreams facilitate the intra-tumoral distribution of tumoral and non-tumoral cells, and the invasion of the normal brain. These fascicles are defined by a specific molecular signature that regulates their organization and function. Oncostreams structure and function depend on overexpression of COL1A1. COL1A1 is a central gene in the dynamic organization of glioma mesenchymal transformation, and a powerful regulator of glioma malignant behavior. Inhibition of COL1A1 eliminated oncostreams, reprogramed the malignant histopathological phenotype, reduced expression of the mesenchymal associated genes, and prolonged animal survival. Oncostreams represent a novel pathological marker of potential value for diagnosis, prognosis, and treatment.

INTRODUCTION

High grade gliomas (HGG) are the most prevalent and malignant brain tumors. They grow rapidly, invade surrounding normal brain, and recur within 12 months. Median survival is 18-20 months, in spite of current standard of care[1,2]. Despite some notable successful outcomes from the large cancer sequencing programs, which identified driver genes in a number of cancers, there have not been major therapeutically actionable breakthroughs in HGG[3-7].

HGG are highly heterogeneous at the cellular, histological and molecular level. Heterogeneity of HGG is illustrated in addition, by characteristic pathological structures such as pseudopalisades, microvascular proliferation, and areas of hypoxia and necrosis[2,8]. The molecular characterization of glioma heterogeneity identified three main molecular signatures: proneural, mesenchymal, and classical[4,9] . However, later studies demonstrated that all three transcriptomic signatures are expressed within individual tumors[5,10,11]. Rather than outright glioma subtypes, the consensus proposes that individual tumors are enriched in particular molecular subtypes. Thus, studies have correlated histological features with genetic alterations and transcriptional expression patterns. For example, highly aggressive histological features such as hypoxic, perinecrotic and microvascular proliferative zones have been associated with the mesenchymal molecular signature and worse prognosis[8]. However, the molecular classification has only minor clinical impact. Thus, alternative classification schemes using a pathway based classification are currently being considered[12]. How these new classifications will deal with tumor heterogeneity remains to be explored.

Tumoral mesenchymal transformation is a hallmark of gliomas[13-15]. A mesenchymal phenotype is defined by cells with spindle-like, fibroblast-like morphology associated with alterations in their dynamic cellular organization leading to an increase in cell migration and invasion[16,17]. The mesenchymal phenotype is controlled by particular transcription factors, and downstream genes related to the extracellular matrix (ECM), cell adhesion, migration, and tumor angiogenesis[15,18,19]. However, the cellular and molecular mechanisms that regulate mesenchymal transformation in gliomas has remained elusive. Integrating morphological features, spatially resolved transcriptomics and cellular dynamics resulting from mesenchymal transformation, growth and invasion are thus of great relevance to our understanding of glioma progression.

Cell migration is essential to continued cancer growth and invasion. Morphological and biochemical changes that occur during mesenchymal transformation allow glioma cells to move throughout the tumor microenvironment and invade the normal brain adjacent to the tumors. Tumor cells can also migrate along blood vessels, white matter tracks, and the subpial surface. Within the tumor microenvironment, aligned extracellular matrix fibers help guide the movement of highly motile mesenchymal-like cancer cells [20-22].

Our study reveals that malignant gliomas, both high grade human gliomas and mouse glioma models, display regular distinctive anatomical multicellular fascicles of aligned and elongated, spindle-like cell. We suggest they are areas of mesenchymal transformation. For the sake of simplicity in their description throughout the manuscript, we have named these areas 'oncostreams'.

Using time lapse laser scanning confocal imaging of high grade glioma explants we demonstrated that oncostreams are organized collective dynamic structures; they are present at the tumor core and at areas of tumor invasion of the normal brain. Collective motion is a form of collective behavior where individual units' (cells) movement is regulated by local intercellular interactions (i.e., attraction/repulsion) resulting in large scale coordinated cellular migration [23-27]. Collective motion plays an essential role in embryogenesis and wound healing[24,28-30]. Emergent organized collective motion patterns could help explain so far poorly understood tumoral behaviors such as invasion, metastasis, and especially in the core of gliomas recurrence[24,28].

Studies of tumor motility have concentrated on the behavior of glioma cells at the tumor invasive border[24,31,32]. Potential motility at the glioma core has not been studied in much detail so far. This study challenges the conventional belief that cells in the central core are non-motile and indicate that the glioma core displays collective migratory patterns. This would suggest that the capacity of gliomas to invade and grow is not only a result of phenomena occurring at the tumor invasive border, but are a result of the overall capacity of gliomas to organize collective motion throughout, from the tumor core to the tumor invasive border.

To study the molecular mechanisms underlying oncostream organization and function we used laser capture microdissection (LCM) followed by RNA-sequencing and bioinformatics analysis. We discovered that oncostreams are defined by a mesenchymal transformation signature enriched in extracellular matrix related proteins, and which suggest that Collagen1A1 (COL1A1)

is a key determinant of oncostream organization. Inhibition of COL1A1 within glioma cells lead to oncostream loss and reshaping of the highly aggressive phenotype of HGG. These data indicate that COL1A1 is likely to both constitute the scaffold of the tumor microenvironment, and to serve to organize areas of collective motion in gliomas.

COL1A1 has been shown previously to be a major component of the extracellular matrix in different cancers, including glioma, and has been reported to promote tumor growth and invasion. Alternatively, some data suggest that collagen fibers could be passive barriers to resist tumor cell infiltration or provide biophysical and biochemical support for cell migration. Some studies reported that density of COL1A1 inversely correlates with glioma patient's prognosis. However, other studies showed that either increased or decreased deposition of collagen could be associated with increased tumor malignancy. Therefore, it is important to further determine the role of COL1A1 in glioma invasion and continued growth.

This study provides a comprehensive study of the histological, morphological, and dynamic properties of glioma tumors. In addition, we uncover a novel characterization of the molecular mechanisms that define intra-tumoral mesenchymal transformation in gliomas and discuss their therapeutic implications. Oncostreams are anatomically and molecularly distinctive, regulate glioma growth and invasion, display collective motion and are regulated by the extracellular matrix, specially by COL1A1. Inhibiting COL1A1 within glioma cells is a potential therapeutic strategy to mitigate glioma mesenchymal transformation, intra-tumoral heterogeneity, and thus, reduce deadly glioma invasion and continued growth.

RESULTS

Intra-tumoral multicellular fascicles of elongated and aligned cells in gliomas

High grade gliomas (HGG) are characterized by anatomical, cellular and molecular heterogeneity which determines, in part, tumor aggressiveness and reduces treatment efficacy[5,7,11]. Histopathological analysis of mouse and human gliomas revealed the presence of frequent distinct multicellular fascicles of elongated (spindle-like) and aligned cells (≈5-30 cells wide) distributed throughout the tumors. These structures resemble areas of mesenchymal transformation which we describe as "oncostreams" (**Fig. 1A-B**).

To study the presence and morphological characterization of oncostreams, we examined histological sections from various mouse glioma models as well as human glioma specimens **(Fig. 1 A-B).** We determined the existence of oncostreams in genetically engineered mouse models (GEMM) of glioma including NPA (Nras, shP53, shATRx) and NPD (Nras, shP53, PDGFβ) and other implantable models (GL26) (**Fig. 1A and Supplementary Fig. 1A**). Moreover, human glioma samples from primary resections and a xenograft glioma model, SJGBM2, established the presence of these multicellular structures in human tissue (**Fig. 1B and Supplementary Fig. 1A**). Morphological analysis characterized that cells within histological areas corresponding to oncostreams have an aspect ratio of 2.63±0.19 (elongated or spindle-like cells) compared to the surrounding tissue where cells have an aspect ratio of 1.37±0.12 (round cells), both in mouse and human gliomas as shown in **Fig. 1C and Supplementary Fig. 1B.** We also determined that elongated cells within oncostreams are nematically aligned with each other, whereas outside of oncostreams, cell orientations are not aligned (**Fig. 1D and Supplementary Fig. 1C).**

To gain insight into the cellular features of oncostreams we asked if they are homogeneous or heterogeneous multicellular structures. We observed that in mouse and human HHG tumors, oncostreams are formed by GFP+ and Sox2+ tumor cells, and also by other cells such as Nestin+ cells, GFAP+ glial derived cells, Iba1+ microglia/macrophages cells, and ACTA2+ mesenchymal cells (**Fig. 1, E and G, and Supplementary Fig. 2 A-C**). Non-tumoral cells within oncostreams were positive aligned with tumor cells in mouse and human HHG (**Fig. 1F and 1G**). Conversely, we detected that low grade gliomas (LGG) exhibited homogenous round cells, and GFAP+ and Iba1+ cells throughout the tumor. These cells did not show any particular orientation or alignment (**Fig. 1H**). This suggests that the relationship of oncostream features with glioma histological grades ought to be further explored.

To test if oncostreams form along existing brain structures, we evaluated their co-localization with white matter tracts. Although, occasional positive immune-reactivity (Neurofilament-L) was present within some areas of the tumors, oncostreams fascicles were not preferentially organized along brain axonal pathways **(Fig. S1D)**. These data indicate that oncostreams are fascicles of spindle-like aligned cells within glioma tumors, which contain tumor and non-tumor cells.

Oncostream density positively correlates with tumor aggressiveness and poor prognosis in mouse and human gliomas

Oncostreams are unique histological features that contribute to intra-tumoral heterogeneity suggesting a potential role in glioma progression and malignancy. To understand whether the presence of oncostreams correlates with tumor aggressiveness and clinical outcomes, we generated genetically engineered tumors of different malignant behaviors using the Sleeping Beauty Transposon system **(Fig. 2A)**. These models reproduce the malignant histopathological features of gliomas as demonstrated in previous studies[33-36]. We induced tumors harboring two different genotypes: (1) Activation of RTK/RAS/PI3K pathway, in combination with p53 and ATRX downregulation (**NPA**), and, (2) RTK/RAS/PI3K activation, p53 downregulation, ATRX downregulation, and mutant IDH1-R132 expression (**NPAI**) **(Fig. 2A)**. IDH1-wild-type tumors (**NPA**) display a highly malignant phenotype and worse survival prognosis (Medial survival (MS): 70 days), compared with tumors harboring the IDH1-R132R mutation, **NPAI,** (MS: 213 days) **(Fig. 2B)**. This outcome reproduces human disease, as patients with IDH1-mutant tumors also have prolonged median survival[1,36,37]. Tumor histopathological analysis showed a positive correlation between the density of oncostreams and tumor malignancy **(Fig. 2C- D)**. NPA (IDH1-WT) tumors exhibited larger areas of oncostreams within a highly infiltrative and heterogeneous glioma characterized by abundant necrosis, microvascular proliferation, pseudopalisades and cellular heterogeneity as described before [35,36]. Conversely, NPAI (IDH1-Mut) tumors display very low densities of oncostreams and a homogenous histology mainly comprised of round cells, low amounts of necrosis, no microvascular proliferation, absence of pseudopalisades and less invasive borders **(Fig. 2C and Supplementary Fig. 5).**

Further, to objectively identify and quantify tumor areas covered by oncostreams, we trained a fully convolutional neural network (fCNN) (**Fig. 2C and Supplementary Fig. 3 and 4A**). Our deep learning analysis found that oncostreams occupied 15.28 ± 6.105% of the area in NPA tumors compared with only 1.18 ± 0.81 % in NPAI tumors (**Fig. 3C and D, and Fig. Supplementary 5A and B**). Cellular alignment analysis validated the presence or absence of oncostreams (**Fig. 3E**).

To determine whether oncostreams are linked to glioma aggressiveness in human patients, we evaluated a large cohort of TCGA glioma diagnostic slides from the Genomic Data Commons Portal of the National Cancer Institute. We visually examined 100 TCGA-glioblastoma multiforme

tissue sections (WHO Grade IV) and 120 TCGA-low grade glioma tissues (WHO Grade II and III) using the portal's slide image viewer (**Supplementary Table 1**). Oncostreams were present in 47% of TCGA-GBM grade IV tumor tissues, in 8.6 % of TCGA-LGG grade III, and were absent from TCGA-LGG grade II (**Fig. 2F-G and Supplementary Table 2**), consistent with tumor aggressiveness (http://gliovis.bioinfo.cnio.es)[38]. We then determined the presence of oncostreams across known molecular subtypes of HHG (Grade IV)[4]. We found oncostream fascicles in 59.4% of Mesenchymal (MES), 53.6% of Classical (CL) subtypes and only 26.7% of Proneural (PN) (**Fig. Supplementary 6A**). Finally, we evaluated oncostreams presence related to IDH status and 1p 19q co-deletion in LGG (Grade III). Oncostreams were present in 16.6% of IDH-WT subtype, 5% of IDHmut-non-codel and absent from IDHmut-codel subtype (**Fig. Supplementary 6B)**. These analyses suggest that oncostream presence is higher in Mesenchymal and Classical subtypes and correlates with IDH-WT status, and thus with a poor prognosis.

To validate the histological identification, we examined H&E images using our deep learning algorithm (**Fig. Supplementary 4B**). We observed a strong concordance (>84%) between machine learning and the manual histological identification of oncostreams (**Table Supplementary 3)**. Oncostream presence and their segmentation by deep learning is illustrated in **Fig. 2H and Fig. Supplementary 7 and 8**. Additionally, alignment analysis of glioma cells confirmed the existence of fascicles of elongated, mesenchymal like cells in human gliomas (**Fig. 2I**). Thus, our deep learning algorithm validates our histological identification of oncostreams and confirms that the density of oncostream fascicles positively correlates with glioma aggressiveness.

Oncostreams are defined by a distinctive spatial transcriptome signature

To determine whether oncostreams fascicles are characterized by a specific gene expression profile, we performed a spatially-resolved transcriptomic analysis using laser capture microdissection (LCM) coupled to RNA sequencing (RNA-Seq). Oncostreams were dissected according to their morphological characteristics defined above. Surrounding areas of homogenous rounded cells were selected as non-oncostreams areas (control) (**Fig. 3A**). RNA-Seq analysis detected a set of 43 differentially expressed (DE) genes; 16 genes were upregulated and 27 downregulated within oncostreams (**Fig. 3 B-C and Table Supplementary 4**).

Functional enrichment analysis of DE genes, performed using the I-PathwayGuide platform (Advaita Corporation, MI, USA), showed that False Discovery Rate (FDR) corrected gene ontology (GOs) terms were associated with migration and extracellular matrix biological process. GOs such as “positive regulation of motility” “positive regulation of cell migration”, “collagen catabolic processes” and “extracellular matrix organization” were the most over-represented biological processes (**Fig. 3D and Table Supplementary 5**). The upregulated DE genes within the relevant GOs include: COL1A1, MMP9, MMP10, ACTA2, ADAMTS2, CDH5, CYR61, PLP1 and those downregulated were ENPP2, AKAP12, BDKRB1 (**Fig. 3E and Fig. Supplementary 9**). Significant DE genes shared by related GOs are shown in **Fig. Supplementary 9**. These migration-related GOs biological process enriched within oncostream fascicles display an overexpression of extracellular matrix (ECM)-associated proteins, suggesting a potential role in regulating oncostreams’ migratory properties.

These data indicate that oncostreams can be identified by a specific gene expression set and suggest a distinct role for oncostreams as intra-tumoral mesenchymal migratory assemblies within glioma tumors.

Oncostreams represent histological patterns of intra-tumoral collective motion in gliomas

To study if oncostreams represent migratory structures within glioma tumors, we established a physiologically viable explant brain tumor slice model containing a high density of oncostreams (**Fig. 4A**). The movement of glioma cells expressing green fluorescent protein (GFP) was visualized using time-lapse confocal imagining, and tracked using Fiji’s plug-in Track-Mate **(Fig. 4A-C).**

Migration analyses show complex glioma cell dynamics throughout the tumor core. The glioma tumor core displays groups of cells (zones) moving with similar nematic orientation (**Fig. 4D and Fig. Supplementary 10A**) which represent collective motion[24,26-28]. Velocity angle distribution indicated the existence of three patterns of collective motility shown schematically in **Fig. 4D and F**: in ‘Zone A’ cells don’t have a preferred direction, in ‘Zone B’ cells move in opposite directions (~ 135° and 315°), and in ‘Zone C’ all cells move with a single similar preferred direction (~ 45°) (**Fig. 4D and F).** We named these patterns ‘s*warm*’ (Zone A), ‘*stream*’ (Zone B), or ‘*flock*’ (Zone C) (**Fig. 4G).** They were classified by likelihood analysis: the distribution of the velocity angle is constant in a *swarm* (all velocity angles are equally probable), bi-modal in a *stream* (cells are

moving in equal but opposite directions), and uni-modal in a *flock* (cells move in one direction) (**Fig. 4H)**. These patterns were observed in all tumor slices examined (**Fig. Supplementary 12, 13 and 14**). Average cell speeds differed among the three patterns (**Fig. 4E, and Supplementary 12, 13 and 14**). In the tumor core, swarms moved faster and without any orientation, followed by directionally moving flocks and streams (**Fig Supplementary 20**). To determine which of these collective motion patterns match oncostream histological features, we analyzed H&E sections corresponding to imaged organotypic slices (**Fig. Supplementary 10B).** Cells within histological areas corresponding to *streams* and *flocks* have an aspect ratio of 2.2 and 2.7, respectively, (spindle-like cells), while those within areas corresponding to *swarms* have an aspect ratio of 1.2 (round cells) **(Fig. Supplementary 10C-D)**. Moreover, elongated cells within *streams* and *flocks* are nematically aligned with each other, whereas round cells within *swarms* are not **(Fig. Supplementary 10E).** As predicted by our *in silico* model, [39] these results suggest that cell shape, or eccentricity, is involved in the organization of collective motion patterns (**Fig. Supplementary 10F**). Therefore, taking into account cell shape and alignment, we define that oncostreams are the histological expression of collective motion patterns (*streams* and *flocks*). Notice that only the dynamic analysis of collective motion can differentiate between *streams* and *flocks*. At the histological level both appear as oncostreams.

In collective motion, interactions among individual cells are sufficient to propagate order throughout a larger population[40]. To define if oncostream migration patterns recall organized collective motion behavior, we analyzed the organization of the cells by performing local pair-wise correlation analysis (relative position and pair directional correlation) by tumor zones (**Fig. Supplementary 11A-C**). These analyses indicate the spatial correlation of location and alignment between individual cells. We observed that within *swarms* cells are more separated, as the relative position of the nearby (nearest?) neighbors is 20-40 µm. S*treams* and *flocks* have higher cell density, and the nearby neighbors are closer at 20-30 µm (**Fig. Supplementary 11E and S12, S13, S14**). Pair-wise directional correlation with nearby neighbors showed that cell movement is positively correlated in all patterns at distances between 10-50 *µm*, with higher correlation left-to-right for *streams* (≈0.2), left-to-right/front-to-back for *flocks* (≈0.2-0.4), and a lower correlation for *swarms* (≈0.1) (**Fig. Supplementary 11F and S12, S13, S14).** We ascertained that tumor cells within oncostreams migrate in a highly correlated directional manner ("streams

(↑↓)" and "flocks (↑↑)"), while non-oncostream cells move randomly without directional alignment and less correlated as "swarms". Thus, our analyses strongly indicate that glioma tumor cores are dynamically heterogeneous and display organized collective migratory behavior associated with tumor histological features.

Oncostreams increase the intratumoral spread of tumoral and non-tumoral cells

Pair-wise correlation analysis showed that oncostream glioma cells are moving collectively. To test the underlying nature of collective oncostream motility, we analyzed adherent junction markers. Tumors with oncostreams were negative for E-cadherin, whereas N-cadherin was upregulated (**Fig. Supplementary 15A**), suggesting that these fascicles move in a manner akin to collective migration of mesenchymal cells of the neural crest[30,41]. Additionally, N-cadherin was elevated in TCGA-GBM (Grade IV) tumors compared to TCGA-LGG (Grade III and II). High levels of N-cadherin correlate with lower survival in HGG patients. (**Fig. Supplementary 15B-C**). E-cadherin expression was negative within the tumor and did not have any correlation with tumor grade in the TCGA data (**Fig. Supplementary 15B-C**).

On the other hand, oncostream growth and motility is unlikely to be due to glioma proliferation. BrdU staining showed no differences between oncostream and non-oncostream regions, and in the oncostreams, the mitotic plane was always perpendicular to the main axis as expected **(Fig. Supplementary D-E).**

Collective motion could affect the distribution of other cells within the tumor. Since oncostreams are heterogeneous structures, we inquired about their potential pro-tumoral role in spreading cells throughout the tumor. We designed co-implantation experiments using human glioma stem cells (MSP-12), and highly aggressive and oncostream-forming glioma cells (GL26) co-implanted into immunosuppressed mice. Implantation of MSP12 cells alone generated slow-growing tumors (median survival of 6-8 months). At 21 days post-implantation, MSP-12 cells remained restricted to the injection area with an average distance of 28.9±7.73 µm from the actual injection site. Surprisingly, when MSP12 cells were co-implanted with GL26-citrine cells, MSP-12 cells spread throughout the tumor, moving along oncostreams to much longer distances (83.7±23.74 µm) from the injection site (**Fig. 4I-K**). Cellular cytoplasmic processes from MSP12 cells implanted alone displayed a random distribution. However, in co-implanted tumors, such

processes from MSP12 cells are completely aligned with glioma GL26 cells within oncostreams **(Fig. 4K-L and Fig. Supplementary 15F)**. These results strongly suggest that oncostreams function as intra-tumoral highways facilitating the rapid distribution of slow-moving glioma cells and/or non-tumor cells throughout the tumor mass. These findings could help explain the dispersal of diverse clonal populations as demonstrated in previous studies, supporting a potential role of oncostreams in determining spatial cellular heterogeneity.

Dynamic interactions at the tumor border: oncostreams foster glioma aggressiveness through collective invasion of the normal brain parenchyma

Furthermore, we asked whether oncostreams participate in glioma invasion. The analysis of histological sections showed that multicellular fascicles of elongated and aligned cells are found invading from the tumor border into the normal brain parenchyma (**Fig 5A**). Formation of streams around blood vessels was also observed (**Fig. 5A**). These patterns are also detected using our deep learning methods (**Fig. Supplementary 16A**).

We then used our glioma explant model to analyze the invasion dynamics by time-lapse confocal imaging at the tumor border (**Fig. 5B**). We implanted glioma NPA GFP+ cells into tdTomato (mT/mG) mice so tumor borders could be delineated. We observed that glioma cells that extended from the tumor border to the normal brain parenchyma used different dynamic patterns, moving as isolated random cells and/or as collective migratory structures moving directionally, and resembled oncostream structures similar to those in the tumor core (**Fig. 5C-F and Fig. Supplementary 17-19**).

To objectively distinguish between different dynamic patterns, we determined the velocity angle distribution, and the likelihood that either distribution corresponded to either a *stream*, a *flock*, or a *swarm*. We found *streams* along the perivascular niche or invading brain parenchyma without following any pre-existing brain structures, as well as cells invading as *flocks*, and *swarms* (**Fig. 5 G, and Fig. Supplementary 17-19 A, C and D**). Glioma cells moving along blood vessels or directly into the brain as single cells is consistent with previous studies[10]. The correlation of position and velocity supports the existence of invading collective motion structures (**Fig. S16C-D**).

Our data indicate the existence of a comprehensive framework of collective motion at the glioma border, that is consistent with previous descriptions[31]. Though the patterns observed at the tumor border are similar to those of the tumor core, cell speed differed between the areas. Cells in the tumor core displayed significantly lower average speeds (*stream*: 4.26; *flock*: 5.95, *swarm*: 6.27 µm/hr) compared to cells at the tumor border or those invading the normal parenchyma (*stream*: 7.95; *flock*: 7.55, *swarm*: 8.01 µm/hr) (**Fig. Supplementary 20A-B**). We conclude that oncostreams (*streams* and *flocks*) are organized collective migratory structures that participate in the dynamic organization of the tumor microenvironment within the tumor core and at the tumor invasive border, and facilitate invasion into the normal brain, impacting the malignant behavior of gliomas.

COL1A1 contributes to oncostream organization in high-grade gliomas

Histopathologically, oncostreams are collective dynamic structures with a defined DE gene expression signature. To understand the molecular mechanisms that regulate oncostream organization and function, we identified critical genes using network analysis. Network interactions revealed that COL1A1 is a hub gene, one of the most highly connected nodes, representing a potential regulator of the network's signaling pathways and biological functions (**Fig 6A and Fig. Supplementary 21A**). We found that the most relevant COL1A1 related pathways include: Focal Adhesion, Extracellular Matrix Organization and Integrin Signaling pathways among others (**Fig. Supplementary 21B-C and Table Supplementary 7 and 8**).

To analyze the role of COL1A1 in oncostream organization, we analyzed COL1A1 expression by immunofluorescence analysis. The COL1A1 gene encodes for alpha-1 type I collagen fibers, herein referred to as collagen. We observed that collagen fibers were aligned within oncostreams and overexpressed in more aggressive NPA (IDH1-WT) gliomas compared with NPAI (IDH1-Mut) tumors. COL1A1 expression was significantly lower and only found surrounding blood vessels in NPAI (IDH-Mut) tumors (**Fig. 6B-C**). Correspondingly, human GBM glioma tumors (IDH1-WT) with high oncostream densities showed prominent alignment of collagen fibers along these fascicles and higher COL1A1 expression compared to LGG (IDH1-Mut) (**Fig. 6D and E**).

Moreover, TCGA-glioma data indicate that COL1A1 has differentially higher expression in GBM histological Grade IV. LGG IDH-WT tumors display higher expression of COL1A1 than IDH1-

Mutant. Within the GBM molecular subtype classification[4,9], the Mesenchymal group shows higher expression of COL1A1 than the Proneural and Classical groups (**Fig. Supplementary 22A**); the COL1A1 gene is clearly associated with the mesenchymal subtype. Analysis of patient survival related to COL1A1 expression showed that mesenchymal GBM subtype displayed a significantly shorter survival (MS: 10.4 days) for COL1A1 high tumors, compared to COL1A1 low (MS: 17.9 days) tumors. Classical and Proneural subtypes did not show survival differences associated to COL1A1 expression (**Fig. Supplementary 22B**).

We also determined the participation of collagen fibers in oncostreams invasion. Immunofluorescence analysis showed that collagen fibers are aligned along multicellular fascicles of glioma cells invading of the normal brain. This data shows how collagen fibers serve as scaffolds for collective tumoral cell invasion (**Fig. Supplementary S23**). Thus, oncostreams represent intra-tumoral mesenchymal-like dynamic features organized along collagen fibers.

COL1A1 depletion leads to oncostream loss and increases in median survival

To evaluate the functional role of COL1A1 in oncostreams formation we generated COL1A1-deficient genetically engineered mouse glioma models. We generate COL1A1 wildtype, and COL1A1 knock-down tumors using different genetic backgrounds (**Fig Supplementary 24A-C**). We observed that COL1A1 downregulation increased median survival (MS) (**Fig. 6F and G**). The knockdown of COL1A1 in NPA tumors (NPAshCOL1A1) exhibited an increased survival (MS: 123 days) compared to NPA control tumors (MS: 68 days) (**Fig. 6F**). Similarly, COL1A1 knockdown in NPD tumors harboring PDGFβ ligand upregulation (NPDshCOL1A1), also exhibited an increased median survival (MS: 98 days) compared to the NPD controls (MS: 74 days) (**Fig. 6G**).

To further analyze the effects of COL1A1 downregulation, we evaluated the histopathological features of glioma tumors, quantified oncostream density using deep learning analysis and evaluated COL1A1 expression within glioma tissue (**Fig. 6 H-K**). We observed that NPA tumors with COL1A1 downregulation showed a significant reduction of COL1A1 within tumors, and it was only maintained in small areas surrounding blood vessels (**Fig. 6H-J**). COL1A1 inhibition led to oncostream loss and reprogramming of the histopathological tumoral characteristics as evidenced by homogenous round cell morphology, resembling low grade tumors (**Fig. 6I and 6K**). Downregulation of COL1A1 in NPD tumors appeared less effective, with large areas of remaining

COL1A1 along hypertrophied blood vessels (**Fig. 6H and 6J**). Nonetheless, COL1A1 was downregulated within tumor cells and oncostream dismantling was significant compared to NPD control. Some oncostream areas remained associated to blood vessels correlating with the location of COL1A1 (**Fig. 6I and 6K**). Moreover, inhibition of COL1A1 within glioma cells led to downregulation of fibronectin expression, a mesenchymal associated marker protein (**Fig. Supplementary 24A-F**) that is associated with a more aggressive phenotype.

These preclinical animal models knocked down the expression of COL1A1 from the earliest stages of tumor development. Further, to evaluate the effects of the pharmacological degradation of deposited fibers of collagen in highly malignant tumors we analyzed explants of brain tumor sections treated with collagenase. We observed that collagenase treatment decreased reticular fibers (general collagen staining), reduced COL1A1 expression by disassembling fibers' alignment along tumoral cells and caused oncostreams depletion in a dose response manner (**Fig. Supplementary 25A-D**). These data indicate that oncostream organization and functions are regulated by COL1A1 extracellular matrix protein. COL1A1 knockdown within glioma cells decreased oncostream formation and reprogramed glioma mesenchymal transformation, thus increasing animal survival. COL1A1 inhibition represents a novel approach for future translational development.

DISCUSSION

Mesenchymal transformation is a hallmark of tumor heterogeneity that has been associated with a more aggressive phenotype and therapeutic resistance[13,15,18]. Mesenchymal transformation involves fibroblast-like morphological changes associated with active migration and gain of expression of mesenchymal genes as previously described[18,19].

Herein we present a comprehensive study that defines the morphological, cellular, dynamic and molecular properties of multicellular mesenchymal-like structures within gliomas. These structures are fascicles of aligned spindle-like cells found throughout the tumors, and represent areas of mesenchymal transformation. We interpret these structures to be the histological expression of areas of collective motion of glioma cells. For the sake of simplicity, we have referred to these areas of mesenchymal transformation as oncostreams.

Oncostreams are areas of mesenchymal transformation and are identified histologically as fascicles of aligned and elongated cells. When examined dynamically, we show that tumor cells move by collective motion within the tumor core and at the invading border. The capacity to identify areas of collective motion in histological sections has allowed us to characterize the molecular organization of such dynamic structures. We thus describe the overall molecular mechanisms that govern the organization and function of these structures, and demonstrate the causal role of individual mediators. Surprisingly, we discovered that COL1A1 is central to the structural and dynamic characteristics of oncostreams. Indeed, the loss of COL1A1 expression from tumor cells disrupts the structural and functional characteristics of oncostreams, resulting in a complete loss of mesenchymal areas within gliomas and a reduction in glioma malignant behavior (**Fig. 7**).

The analysis of the gene ontologies over-represented within oncostreams indicates that oncostreams denote areas enriched for "positive regulation of cell migration", and in mesenchymal related genes. Interestingly, COL1A1 appeared as a central hub of oncostream organization and mesenchymal transformation. We postulate that oncostreams are the histopathological expression of patterns of collective motion (i.e., streams and flocks) in high grade glioma tumors. Different strategies of cell migration encountered in our gliomas are reminiscent of migratory characteristics observed during embryonic development[28,29,41]. In developmental biology, collective motion is represented by cells moving together in clusters, sheets, streams, or in other multicellular arrangements[25,28,29].

Our studies of oncostream dynamics at the tumor core are compatible with the results of Ralitza et al. This group studied *ex-vivo* explant slices of spontaneous intestinal carcinoma, and showed that cells within the tumor core were highly dynamic and display directionally correlated cell motion[42], similar to our results described herein. Recent *in silico* based mathematical modelling of glioma cell dynamics by our group, showed that only elongated cells, but not spherical cells, are able to form organized aligned cellular structures in a cell-density dependent manner[39]. Our modeling studies strongly support our *in-vivo* and *ex-vivo* data described in this manuscript.

Moreover, it has been described that increased matrix cross-linking, enzymatic remodeling and parallel orientation of matrix collagen fibers stiffens tissue, modifies cell morphology and promotes cell migration and invasion[43-47]. Our results support the proposal that oncostreams

serve as highways to spread tumor, and non-tumor cells, throughout the tumor. Dispersal of tumor and non-tumoral cells throughout the tumors could help explain the mixing of different clonal populations seen in molecular studies of high-grade gliomas[10].

This study contributes to explaining how a particular feature of intratumoral heterogeneity, namely mesenchymal transformation, affects HGG progression. Our data indicate that the density of oncostreams plays a potential role in overall glioma malignant behavior in mouse and human gliomas.

Spatially resolved transcriptional analysis using laser capture microdissection provided novel insights into the molecular mechanisms that regulate oncostreams functions. Oncostreams were defined by a unique transcriptomic signature that matched our immunochistochemical studies. COL1A1 overexpression within oncostreams was complemented with the overexpression of extracellular matrix proteins such as MMP9, MMP10, ADAMTS2, which are known to remodel and participate in the reorganization of collagen fibers. Oncostream fascicles were correspondingly enriched in COL1A1 when assessed by immunohistochemistry.

Within the extracellular matrix collagen fibers constitute a scaffold for the organization of the tumor microenvironment and thus promote tumor infiltration and invasion. While collagen was previously thought to be a passive barrier that could reduce tumor invasion, it has now been shown that collagen fibers can serve as mechanical and biochemical tracks that facilitate cellular migration and tumor progression[43,45,48,49]. Previously, multi-cancer computational analysis found that within a mesenchymal transformation signature in different cancers including gliomas, COL1A1 was one of the top differentially expressed genes[15,19,50]. COL1A1 is overexpressed in high grade malignant gliomas and its expression levels are inversely correlated with patient survival[51] as indicated in https://www.cancer.gov/tcga. In our mouse glioma models and in human gliomas, tumors with higher density of oncostreams also express higher levels of COL1A1. COL1A1 is a consistently differentially expressed gene in the glioma mesenchymal signature identified in malignant gliomas and in glioma stem cells as described in previous studies[4,9,52]. Overall, our data are in agreement with a recent study by Puchalski *et al.*, which assigned genetic and transcriptional information to the most common morphological hallmarks of a glioma, emphasizing the importance of integrative histo-molecular studies[8].

478 Surprisingly, our data indicate a remarkable plasticity of the mesenchymal phenotype in gliomas.
479 Genetic inhibition of COL1A1 within glioma cells depleted COL1A1 from tumors, eliminated
480 oncostream structures, reduced the glioma malignant phenotype, and prolonged animal survival.
481 Our findings are comparable with results from various studies that investigated the *in-vitro* and
482 *in-vivo* consequences of collagen depletion, inhibition of collagen cross-linking or collagen
483 synthesis inhibition on normalizing tumor ECM. In these studies, inhibition of collagen led to
484 changes in the ECM which improved drug penetration, efficacy, as well as tumor access of
485 therapeutic nano-particles or gene based therapies[53-57]. However, a mayor remodeling of the
486 tumor mesenchymal phenotype in response to inhibition of COL1A1 has not been described
487 earlier.
488 Moreover, in this study we observed that oncostreams fascicles, function as multicellular
489 structures that facilitate tumor cell invasion, and thus further increase glioma aggressiveness.
490 Our data strongly support motility of cancer cells as essential to tumor growth and invasion of
491 normal parenchyma[24,31,32,58,59].
492 In summary, our observations suggest that oncostreams are morphologically and molecularly
493 distinct structures that represent areas of collective motion that contribute to tumor growth and
494 invasion. These malignant dynamic structures overexpress COL1A1. COL1A1 knockdown
495 eliminates oncostreams, reduces the mesenchymal phenotype, and delays tumor progression.
496 Our findings open new paths to understanding tumor mesenchymal transformation and its
497 therapeutic treatment. We propose that depletion of COL1A1 within oncostreams is a promising
498 approach to reprogram mesenchymal transformation in glioma tumor as a novel therapeutic
499 approach, and thus reduce the glioma malignant phenotype.

500

501 **METHODS**

502 **Glioma cell lines and culture conditions:**

503 Mouse glioma cells (NPA, GL26) and human glioma cells (MSP-12, SJGBM2) were maintained at
504 37 °C with 5% CO2 and their respective media as described before[33-36]. Mouse NPA (N-Ras,
505 shp53-GFP and shATRX-GFP) neurospheres were derived from genetically engineered tumor
506 using the Sleeping Beauty (SB) transposase system as previously described[33-36]. Mouse GL26
507 glioma cell were generated by Sugiura K and obtained from the frozen stock maintained by the

508 National Cancer Institute (Bethesda, MD)[22]. MSP-12 human glioma cell lines were provided by
509 Christine Brown, City of Hope, and SJGBM2 human glioma cells were provided by Children's
510 Oncology Group (COG) Repository, Health Science Center, Texas Tech University.

511 **Intracranial implantable syngeneic mouse gliomas:**

512 Glioma tumors were generated by stereotactic intracranial implantation into the mouse striatum
513 of 3.0 x 104 mouse glioma cells (either, NPA, or, GL26) in C57BL/6 mice and human glioma cells
514 in immune-deficient NSG mice (SJGBM2) as described before[34-36,60]. To test whether oncostream
515 tumor cells help move other cells throughout the tumor we generated a co-implantation glioma
516 model by intracranial implantation of highly malignant GL26-citrine cells with low aggressive
517 human MSP12 glioma cells at a ratio of 1:30 (1,000 GL26-citrine cells and 30,000 MSP12 cells) in
518 immune-deficient NSG mice. As controls, NSG mice were implanted with 30,000 MSP12 cells
519 alone or 1,000 GL26-citrine cells alone as controls. Experiments were conducted according to the
520 guidelines approved by the Institutional Animal Care (IACUC) and Use Committee at the
521 University of Michigan. Stereotactic implantation was performed as previously described[34].

522 **Genetically engineered mouse glioma models (GEMM)**

523 We used genetically engineered mouse glioma models for survival analysis and histopathological
524 analysis. Murine glioma tumors harboring different genetic drivers were generated using the
525 Sleeping Beauty (SB) transposon system as described before[33,34,36]. Genetic modifications were
526 induced in postnatal day 1 (P01) male and female wild-type C57BL/6 mice (Jackson Laboratory),
527 according to IACUC regulations. shRNA targeting the COL1A1 gene was cloned as describe in
528 detail in Supplementary Methods.

529 **Analysis of oncostreams in human glioma tissue**

530 Oncostream presence was analyzed in H&E sections of paraformaldehyde-fixed paraffin-
531 embedded (PFPE) human glioma samples obtained from primary surgery from the University of
532 Michigan Medical School Hospital. To determine the presence of oncostreams in a large cohort
533 of human glioma tissues we used the biospecimens from "The Cancer Genome Atlas Research
534 Network" (TCGA) from the Genomic Data Commons Data Portal, National Cancer Institute, NIH
535 (https://portal.gdc.cancer.gov). We analyzed primary Glioblastoma multiforme (TCGA-GBM) and
536 Low-Grade Glioma (TCGA-LGG) databases. We selected cases that have available the Slide Image

537 and diagnostic Slides. The diagnostic slides are available for TCGA-GBM: 389 patients and TCGA-
538 LGG: 491 patients. The presence of oncostreams was scored on 100 TCGA-GBM Grade IV tissue
539 samples and 120 TCGA-LGG samples.

540 **Cell aspect ratio and alignment analysis in H&E tumor sections**

541 Images were obtained using bright-field microscopy of H&E stained paraffin sections (Olympus
542 BX53 Upright Microscope). Tumors were imaged using 40X and 20X objectives. Images were
543 processed using the program ImageJ as indicated in detail in supplementary methods.

544 **Deep learning analysis for oncostreams detection on H&E staining of glioma tissue**

545 A fully convolutional neural network (fCNN) was trained in order to identify and segment
546 oncostreams in histologic images[61]. We implemented a U-Net architecture to provide semantic
547 segmentation of glioma specimens using deep learning[62-64]. Our oncostream dataset consisted of
548 images from sacrificed mice and open-source images from The Cancer Genome Atlas (TCGA). A
549 total of 109 hematoxylin and eosin (H&E) stained histologic mice images and 64 from TCGA were
550 reviewed and oncostreams were manually segmented by the study authors (AC, A.E.A and P.R.L.).
551 Images from both datasets were then augmented by randomly sampling regions within each
552 image to generate unique patches (~ 300 patches/image). The location and scale of each patch
553 was randomly chosen to allow for oncostream segmentation to be scale invariant. The analysis is
554 explained in more detail in Supplementary Methods.

555 **Immunohistochemistry on paraffin embedded brain tumors**

556 This protocol was performed as described before[34] and as is detailed in Supplementary Methods.
557 Primary antibodies were diluted at the concentration indicated in Table Supplementary 8. Images
558 were obtained using bright-field microscopy from five independent biological replicates
559 (Olympus BX53 Upright Microscope). Ten different fields of each section were selected at random
560 for study to include heterogeneous tumor areas. For immunofluorescence on paraffin embedded
561 sections from brain tumors images were acquired with a laser scanning confocal microscope (LSM
562 880, Axio Observer, Zeiss, Germany). Integrated density was determined for the analysis of
563 Col1a1 expression using Image J. For immunohistochemistry on vibratome brain tumor sections
564 were left in 4% paraformaldehyde fixation for 48 hours and then transferred to PBS 0.1% sodium
565 azide for an additional 24 hours at 4°C. A Leica VT100S vibratome was used to obtain 50 µm

566 coronal brain sections. The immunohistochemistry protocol was performed as previously
567 described[65,66].

568 **Laser capture microdissection (LCM) of brain tumors**

569 Malignant glioma tumors were induced by intracranial implantation of NPA neurospheres in
570 C57BL/6 mice as described above. LCM approach to analyze differential mRNA expression of
571 intra-tumoral glioma heterogeneity was performed as described before[67].

572 **RNA-Sequencing and bioinformatics analysis**

573 RNA was isolated for laser microdissected tissues using the RNeasy Plus Micro Kit following the
574 manufacturer recommendations (Qiagen). Before library preparation, RNA was assessed for
575 quality using the TapeStation System (Agilent, Santa Clara, CA) using manufacturer's
576 recommended protocols. We obtained a RIN between 6 to 7 after laser microdissection of glioma
577 tissue. A RIN of 6 was determined to be suitable for cDNA library preparation. 0.25 ng to 10 ng of
578 total RNA was used for cDNA library preparation using a kit suitable for RNA isolation at pico-
579 molar concentrations (MARTer Stranded Total RNA-Seq Kit v2 - Pico Input Mammalian) following
580 manufacturer recommended protocol (Clontech/Takara Bio #635005). Sequencing was
581 performed by the UM DNA Sequencing Core, using the Illumina Hi-Seq platform and
582 Bioinformatic analysis were executed by the UM Bioinformatics Core. Differentially expressed
583 genes of all tumors were used for gene ontology (GO), Pathways analysis and genes analysis using
584 iPathwayGuide (Advaita Corporation 2021). Network analysis of the DE genes were achieved
585 using Cytoscape and Reactome App. Network was clustered by Reactome Functional Interaction
586 (FI). Analysis of the expression of COL1A1 in normal tissue and in human glionas were performed
587 using the dataset of TCGA-GBM and TCGA-LGG from Gliovis (http://gliovis.bioinfo.cnio.es)[38].

588 **Tumor explant brain slice culture glioma model and time-lapse confocal imaging:**

589 For the analysis of glioma dynamic, we generated tumors by intracranial implantation of 3 x 104
590 NPA neurospheres which were used to carry out a 3D explant slice culture glioma model. C57BL6
591 animals were used dynamic analysis in the tumor core and B6.129(Cg)-Gt(ROSA)26Sortm4(ACTB-
592 tdTomato,-EGFP)Luo/J- transgenic mice (Jackson laboratory, STOCK 007676) were used for
593 invasion analysis. Mice were euthanized at 19 days' post-implantation. Brains were removed,
594 dissected, and embedded in a 4% agarose solution and kept on ice for 5 minutes. Then, brains

were submerged in ice-cold and oxygenated media (DMEM High-Glucose without phenol red, GibcoTM, USA) and sectioned in a Leica VT100S vibratome (Leica, Buffalo Grove, IL) set to 300 µm in the z-direction. All steps were performed under sterile conditions in a BSL2 laminar flow hood. Brain tumor sections were transferred to laminin-coated Millicel Cell Culture Insert (PICM0RG50, Millipore Sigma, USA). Tumor slices were maintained in D-MEM F-12 media supplemented with 25% FBS, Penicillin-Streptomycin 10.000 U/ML at 37 °C with a 5% CO2 atmosphere for 24 hours. After 24 hours' media was replaced for DMEM-F12 media supplemented with B27 2%, N2 1%, Normocin 0.2 %, Penicillin-Streptomycin 10.000 U/ML and growth factors EGF and FGF 40 ng/ml. For time-lapse imaging slices were placed in an incubator chamber of a single photon laser scanning confocal microscope model LSM 880 (Carl Zeiss, Jena, Germany) at 37 °C with a 5% CO2. Images were obtained every ten minutes for 100-300 cycles. Following movie acquisition, sections were fixed in 4% paraformaldehyde (PFA) for 2 days. Fixed sections were embedded in 2% agarose for H&E and immunohistochemistry analysis. Sections were processed and embedded in paraffin at the University of Michigan Microscopy & Image Analysis Core Facility using a Leica ASP 300 paraffin tissue processor/Tissue-Tek paraffin tissue embedding station (Leica, Buffalo Grove IL). Tumor explant were used for collagenase treatment. Sections were then treated for 48 hours with collagenase (C2399, MilliporeSigma, USA) at a concentration of 5, 10, or 15 units/ml or vehicle control. Following treatment, sections were fixed in 4% paraformaldehyde (PFA) for 2 days.

Mathematical analysis of tumor cell movement

To determine the movement of cells in different areas of the tumor we performed localized statistical analysis in different zones of the tumor. We selected localized areas based on the organization of cells in clusters, group of cells moving together with similar distribution. Raw data of 4 movies from the tumor core and 4 movies from the tumor border were analyzed for 293 cycles (core) and 186 cycles (border) for a frame rate of $\Delta t = 10$ min per image. To track the evolution of cells motion, we used the software Fiji with the plugin Track-Mate. Analysis was performed as indicated in detail in Supplementary Methods.

Classification of glioma migration patterns

To classify the collective cellular motion behavior of the three type of patterns called flock, stream and swarm illustrated in Supplementary Figure S10F we used as criteria the orientation of each cell described by its unique velocity angle denoted θi. More precisely, we transformed the Angle Velocity Distribution graph into a histogram where we examined the distribution of all the values θi. A schematic representation of these distributions is depicted in Figure 4G. Considering a data-set θn n=1…N of orientations where N is the total number of cells, $\theta n \in [0, 2\pi]$ is the direction of the cell n. We tested three types of distributions ρ to describe the dataset and give a likelihood in each case as described in Supplementary Methods. The Akaiki Weight (AW) indicates which pattern has the highest likelihood in each experimental situation.

Statistical Analysis:

All in vivo experiments were performed using independent biological replicates, as indicated in the text and figures for each experiment. Data are shown as the mean ± SEM. Any difference was considered statistically significant when $p < 0.05$ using the ANOVA test. In experiments that included one variable, the one-way ANOVA test was used. In experiments with two independent variables, the two-way ANOVA test was employed. A posterior Tukey's multiple comparisons test was used for mean comparisons. Student t-test was used to compare unpaired data from two samples. Survival data were entered into Kaplan-Meier survival curves plots, and statistical analysis was performed using the Mantel log-rank test. The effect size is expressed in median survival (MS). Significance was determined if $p<0.05$. All analyses were conducted using GraphPad Prism (version 8.0.0) or SAS (2021 SAS Institute, Cary, NC). Each statistical test used is indicated within the figure legends.

Data availability: All data is available in the main text or the supplementary information.

REFERENCES

1 Parsons, D. W. *et al.* An integrated genomic analysis of human glioblastoma multiforme. *Science (New York, N.Y.)* **321**, 1807-1812, doi:10.1126/science.1164382 (2008).

2 Louis, D. N. *et al.* The 2007 WHO Classification of Tumours of the Central Nervous System. *Acta Neuropathologica* **114**, 97-109, doi:10.1007/s00401-007-0243-4 (2007).

3 Ceccarelli, M. *et al.* Molecular Profiling Reveals Biologically Discrete Subsets and Pathways of Progression in Diffuse Glioma. *Cell* **164**, 550-563, doi:10.1016/j.cell.2015.12.028 (2016).

4 Verhaak, R. G. *et al.* Integrated genomic analysis identifies clinically relevant subtypes of glioblastoma characterized by abnormalities in PDGFRA, IDH1, EGFR, and NF1. *Cancer Cell* **17**, 98-110, doi:10.1016/j.ccr.2009.12.020 (2010).

5 Sottoriva, A. *et al.* Intratumor heterogeneity in human glioblastoma reflects cancer evolutionary dynamics. *Proceedings of the National Academy of Sciences of the United States of America* **110**, 4009-4014, doi:10.1073/pnas.1219747110 (2013).

6 Brennan, C. W. *et al.* The somatic genomic landscape of glioblastoma. *Cell* **155**, 462-477, doi:10.1016/j.cell.2013.09.034 (2013).

7 Nicholson, J. G. & Fine, H. A. Diffuse Glioma Heterogeneity and Its Therapeutic Implications. *Cancer discovery* **11**, 575-590, doi:10.1158/2159-8290.Cd-20-1474 (2021).

8 Puchalski, R. B. *et al.* An anatomic transcriptional atlas of human glioblastoma. *Science (New York, N.Y.)* **360**, 660-663, doi:10.1126/science.aaf2666 (2018).

9 Wang, Q. *et al.* Tumor Evolution of Glioma-Intrinsic Gene Expression Subtypes Associates with Immunological Changes in the Microenvironment. *Cancer Cell* **32**, 42-56.e46, doi:10.1016/j.ccell.2017.06.003 (2017).

10 Patel, A. P. *et al.* Single-cell RNA-seq highlights intratumoral heterogeneity in primary glioblastoma. *Science (New York, N.Y.)* **344**, 1396-1401, doi:10.1126/science.1254257 (2014).

11 Bergmann, N. *et al.* The Intratumoral Heterogeneity Reflects the Intertumoral Subtypes of Glioblastoma Multiforme: A Regional Immunohistochemistry Analysis. *Front Oncol* **10**, 494, doi:10.3389/fonc.2020.00494 (2020).

12 Garofano, L. *et al.* Pathway-based classification of glioblastoma uncovers a mitochondrial subtype with therapeutic vulnerabilities. *Nat Cancer* **2**, 141-156, doi:10.1038/s43018-020-00159-4 (2021).

13 Kim, Y. *et al.* Perspective of mesenchymal transformation in glioblastoma. *Acta Neuropathol Commun* **9**, 50, doi:10.1186/s40478-021-01151-4 (2021).

14 Azam, Z., To, S. T. & Tannous, B. A. Mesenchymal Transformation: The Rosetta Stone of Glioblastoma Pathogenesis and Therapy Resistance. *Adv Sci (Weinh)* **7**, 2002015, doi:10.1002/advs.202002015 (2020).

15 Behnan, J., Finocchiaro, G. & Hanna, G. The landscape of the mesenchymal signature in brain tumours. *Brain* **142**, 847-866, doi:10.1093/brain/awz044 (2019).

16 Yang, J. *et al.* Guidelines and definitions for research on epithelial-mesenchymal transition. *Nat Rev Mol Cell Biol* **21**, 341-352, doi:10.1038/s41580-020-0237-9 (2020).

17 Williams, E. D., Gao, D., Redfern, A. & Thompson, E. W. Controversies around epithelial-mesenchymal plasticity in cancer metastasis. *Nat Rev Cancer* **19**, 716-732, doi:10.1038/s41568-019-0213-x (2019).

18 Carro, M. S. *et al.* The transcriptional network for mesenchymal transformation of brain tumours. *Nature* **463**, 318-325, doi:10.1038/nature08712 (2010).

19 Cheng, W. Y., Kandel, J. J., Yamashiro, D. J., Canoll, P. & Anastassiou, D. A multi-cancer mesenchymal transition gene expression signature is associated with prolonged time to recurrence in glioblastoma. *PLoS One* **7**, e34705, doi:10.1371/journal.pone.0034705 (2012).

20 Ray, A., Morford, R. K., Ghaderi, N., Odde, D. J. & Provenzano, P. P. Dynamics of 3D carcinoma cell invasion into aligned collagen. *Integr Biol (Camb)* **10**, 100-112, doi:10.1039/c7ib00152e (2018).

21 Pickup, M. W., Mouw, J. K. & Weaver, V. M. The extracellular matrix modulates the hallmarks of cancer. *EMBO Rep* **15**, 1243-1253, doi:10.15252/embr.201439246 (2014).

22 Baker, G. J. *et al.* Mechanisms of glioma formation: iterative perivascular glioma growth and invasion leads to tumor progression, VEGF-independent vascularization, and resistance to antiangiogenic therapy. *Neoplasia* **16**, 543-561, doi:10.1016/j.neo.2014.06.003 (2014).

23 Deisboeck, T. S. & Couzin, I. D. Collective behavior in cancer cell populations. *Bioessays* **31**, 190-197, doi:10.1002/bies.200800084 (2009).
24 Friedl, P., Locker, J., Sahai, E. & Segall, J. E. Classifying collective cancer cell invasion. *Nat Cell Biol* **14**, 777-783, doi:10.1038/ncb2548 (2012).
25 Friedl, P. & Mayor, R. Tuning Collective Cell Migration by Cell-Cell Junction Regulation. *Cold Spring Harb Perspect Biol* **9**, doi:10.1101/cshperspect.a029199 (2017).
26 Méhes, E. & Vicsek, T. Collective motion of cells: from experiments to models. *Integr Biol (Camb)* **6**, 831-854, doi:10.1039/c4ib00115j (2014).
27 Rørth, P. Fellow travellers: emergent properties of collective cell migration. *EMBO Rep* **13**, 984-991, doi:10.1038/embor.2012.149 (2012).
28 Friedl, P. & Gilmour, D. Collective cell migration in morphogenesis, regeneration and cancer. *Nat Rev Mol Cell Biol* **10**, 445-457, doi:10.1038/nrm2720 (2009).
29 Scarpa, E. & Mayor, R. Collective cell migration in development. *J Cell Biol* **212**, 143-155, doi:10.1083/jcb.201508047 (2016).
30 Theveneau, E. & Mayor, R. Neural crest delamination and migration: from epithelium-to-mesenchyme transition to collective cell migration. *Dev Biol* **366**, 34-54, doi:10.1016/j.ydbio.2011.12.041 (2012).
31 Alieva, M. *et al.* Intravital imaging of glioma border morphology reveals distinctive cellular dynamics and contribution to tumor cell invasion. *Scientific reports* **9**, 2054, doi:10.1038/s41598-019-38625-4 (2019).
32 Haeger, A., Krause, M., Wolf, K. & Friedl, P. Cell jamming: collective invasion of mesenchymal tumor cells imposed by tissue confinement. *Biochim Biophys Acta* **1840**, 2386-2395, doi:10.1016/j.bbagen.2014.03.020 (2014).
33 Calinescu, A. A. *et al.* Transposon mediated integration of plasmid DNA into the subventricular zone of neonatal mice to generate novel models of glioblastoma. *Journal of visualized experiments : JoVE*, doi:10.3791/52443 (2015).
34 Comba, A. *et al.* Fyn tyrosine kinase, a downstream target of receptor tyrosine kinases, modulates antiglioma immune responses. *Neuro-oncology* **22**, 806-818 (2020).
35 Koschmann, C. *et al.* ATRX loss promotes tumor growth and impairs nonhomologous end joining DNA repair in glioma. *Sci Transl Med* **8**, 328ra328, doi:10.1126/scitranslmed.aac8228 (2016).
36 Núñez, F. J. *et al.* IDH1-R132H acts as a tumor suppressor in glioma via epigenetic up-regulation of the DNA damage response. **11**, eaaq1427, doi:10.1126/scitranslmed.aaq1427 %J Science Translational Medicine (2019).
37 Brat, D. J. *et al.* Comprehensive, Integrative Genomic Analysis of Diffuse Lower-Grade Gliomas. *N Engl J Med* **372**, 2481-2498, doi:10.1056/NEJMoa1402121 (2015).
38 Bowman, R. L., Wang, Q., Carro, A., Verhaak, R. G. & Squatrito, M. GlioVis data portal for visualization and analysis of brain tumor expression datasets. *Neuro-oncology* **19**, 139-141, doi:10.1093/neuonc/now247 (2017).
39 Jamous, S., Comba, A., Lowenstein, P. R. & Motsch, S. Self-organization in brain tumors: How cell morphology and cell density influence glioma pattern formation. *PLoS computational biology* **16**, e1007611 (2020).
40 Bialek, W. *et al.* Statistical mechanics for natural flocks of birds. *Proceedings of the National Academy of Sciences of the United States of America* **109**, 4786-4791, doi:10.1073/pnas.1118633109 (2012).
41 Szabó, A. & Mayor, R. Mechanisms of Neural Crest Migration. *Annu Rev Genet* **52**, 43-63, doi:10.1146/annurev-genet-120417-031559 (2018).
42 Staneva, R. *et al.* Cancer cells in the tumor core exhibit spatially coordinated migration patterns. *Journal of cell science* **132**, doi:10.1242/jcs.220277 (2019).

751 43 Fang, M., Yuan, J., Peng, C. & Li, Y. Collagen as a double-edged sword in tumor progression.
752 *Tumour Biol* **35**, 2871-2882, doi:10.1007/s13277-013-1511-7 (2014).
753 44 Payne, L. S. & Huang, P. H. The pathobiology of collagens in glioma. *Mol Cancer Res* **11**, 1129-
754 1140, doi:10.1158/1541-7786.MCR-13-0236 (2013).
755 45 Brett, E. A., Sauter, M. A., Machens, H. G. & Duscher, D. Tumor-associated collagen signatures:
756 pushing tumor boundaries. *Cancer Metab* **8**, 14, doi:10.1186/s40170-020-00221-w (2020).
757 46 Egeblad, M., Rasch, M. G. & Weaver, V. M. Dynamic interplay between the collagen scaffold and
758 tumor evolution. *Curr Opin Cell Biol* **22**, 697-706, doi:10.1016/j.ceb.2010.08.015 (2010).
759 47 Provenzano, P. P. *et al.* Collagen reorganization at the tumor-stromal interface facilitates local
760 invasion. *BMC Med* **4**, 38, doi:10.1186/1741-7015-4-38 (2006).
761 48 Mammoto, T. *et al.* Role of collagen matrix in tumor angiogenesis and glioblastoma multiforme
762 progression. *Am J Pathol* **183**, 1293-1305, doi:10.1016/j.ajpath.2013.06.026 (2013).
763 49 Shintani, Y., Hollingsworth, M. A., Wheelock, M. J. & Johnson, K. R. Collagen I promotes
764 metastasis in pancreatic cancer by activating c-Jun NH(2)-terminal kinase 1 and up-regulating N-
765 cadherin expression. *Cancer research* **66**, 11745-11753, doi:10.1158/0008-5472.CAN-06-2322
766 (2006).
767 50 Kim, H., Watkinson, J., Varadan, V. & Anastassiou, D. Multi-cancer computational analysis
768 reveals invasion-associated variant of desmoplastic reaction involving INHBA, THBS2 and
769 COL11A1. *BMC Med Genomics* **3**, 51, doi:10.1186/1755-8794-3-51 (2010).
770 51 Glioma through the looking GLASS: molecular evolution of diffuse gliomas and the Glioma
771 Longitudinal Analysis Consortium. *Neuro-oncology* **20**, 873-884, doi:10.1093/neuonc/noy020
772 (2018).
773 52 Behnan, J. *et al.* Differential propagation of stroma and cancer stem cells dictates tumorigenesis
774 and multipotency. *Oncogene* **36**, 570-584, doi:10.1038/onc.2016.230 (2017).
775 53 Dolor, A. & Szoka, F. C., Jr. Digesting a Path Forward: The Utility of Collagenase Tumor
776 Treatment for Improved Drug Delivery. *Mol Pharm* **15**, 2069-2083,
777 doi:10.1021/acs.molpharmaceut.8b00319 (2018).
778 54 Diop-Frimpong, B., Chauhan, V. P., Krane, S., Boucher, Y. & Jain, R. K. Losartan inhibits collagen I
779 synthesis and improves the distribution and efficacy of nanotherapeutics in tumors. *Proceedings*
780 *of the National Academy of Sciences of the United States of America* **108**, 2909-2914,
781 doi:10.1073/pnas.1018892108 (2011).
782 55 Kumar, S., Henning-Knechtel, A., Magzoub, M. & Hamilton, A. D. Peptidomimetic-Based
783 Multidomain Targeting Offers Critical Evaluation of Aβ Structure and Toxic Function. *J Am Chem*
784 *Soc* **140**, 6562-6574, doi:10.1021/jacs.7b13401 (2018).
785 56 Kato, M., Hattori, Y., Kubo, M. & Maitani, Y. Collagenase-1 injection improved tumor distribution
786 and gene expression of cationic lipoplex. *Int J Pharm* **423**, 428-434,
787 doi:10.1016/j.ijpharm.2011.12.015 (2012).
788 57 Lee, S. *et al.* Extracellular matrix remodeling in vivo for enhancing tumor-targeting efficiency of
789 nanoparticle drug carriers using the pulsed high intensity focused ultrasound. *J Control Release*
790 **263**, 68-78, doi:10.1016/j.jconrel.2017.02.035 (2017).
791 58 Gritsenko, P. G. & Friedl, P. Adaptive adhesion systems mediate glioma cell invasion in complex
792 environments. *Journal of cell science* **131**, doi:10.1242/jcs.216382 (2018).
793 59 Gritsenko, P. G. *et al.* p120-catenin-dependent collective brain infiltration by glioma cell
794 networks. *Nat Cell Biol* **22**, 97-107, doi:10.1038/s41556-019-0443-x (2020).
795 60 Kamran, N. *et al.* Current state and future prospects of immunotherapy for glioma.
796 *Immunotherapy* **10**, 317-339, doi:10.2217/imt-2017-0122 (2018).
797 61 Shelhamer, E., Long, J. & Darrell, T. Fully Convolutional Networks for Semantic Segmentation.
798 *IEEE Trans Pattern Anal Mach Intell* **39**, 640-651, doi:10.1109/tpami.2016.2572683 (2017).
799 62 Ronneberger, O., Fischer, P. & Brox, T. (2018).

63 Sharma, M., Pachori, R. & Acharya, U. R. Adam: a method for stochastic optimization. *Pattern Recognit. Lett* **94**, 172-179 (2017).
64 Hollon, T. C. *et al.* Near real-time intraoperative brain tumor diagnosis using stimulated Raman histology and deep neural networks. *Nat Med* **26**, 52-58, doi:10.1038/s41591-019-0715-9 (2020).
65 Wilson, T. J., Zamler, D. B., Doherty, R., Castro, M. G. & Lowenstein, P. R. Reversibility of glioma stem cells' phenotypes explains their complex in vitro and in vivo behavior: Discovery of a novel neurosphere-specific enzyme, cGMP-dependent protein kinase 1, using the genomic landscape of human glioma stem cells as a discovery tool. *Oncotarget* **7**, 63020-63041, doi:10.18632/oncotarget.11589 (2016).
66 Yadav, V. N. *et al.* CXCR4 increases in-vivo glioma perivascular invasion, and reduces radiation induced apoptosis: A genetic knockdown study. *Oncotarget* **7**, 83701-83719, doi:10.18632/oncotarget.13295 (2016).
67 Comba, A. *et al.* Laser Capture Microdissection of Glioma Subregions for Spatial and Molecular Characterization of Intratumoral Heterogeneity, Oncostreams, and Invasion. *JoVE (Journal of Visualized Experiments)*, e60939 (2020).

ACKNOWLEDGMENTS

We thank all members of our laboratory for advice and comments on this work. This work was supported by National Institutes of Health, National Institute of Neurological Disorders and Stroke (NIH/NINDS) grants: R37-NS094804, R01-NS105556, R21-NS107894, R21-NS091555; R01-NS074387 to M.G.C.; National Institute of Neurological Disorders and Stroke (NIH/NINDS) grants: R01-NS076991, R01-NS096756, R01-NS082311 to P.R.L.; National Institute of Biomedical Imaging and Bioengineering (NIH/NIBI): R01-EB022563; National Cancer Institute (NIH/NCI) U01CA224160; Rogel Cancer Center at The University of Michigan G023089 to M.G.C. Ian's Friends Foundation grant G024230, Leah's Happy Hearts Foundation grant G013908, Pediatric Brain Tumor Foundation grant G023387 and ChadTough Foundation grant G023419 to P.R.L. RNA Biomedicine grant: F046166 to M.G.C. Health and Human Services, National Institutes of Health, UL1 TR002240 to Michigan Institute for Clinical and Health Research (MICHR), Postdoctoral Translational Scholars Program (PTSP), Project F049768 to A.C.

AUTHORS INFORMATION

Affiliations:

Dept. of Neurosurgery, University of Michigan Medical School, Ann Arbor, 48109, MI, USA
Andrea Comba, Patrick J. Dunn, Todd C. Hollon, Daniel B. Zamler, Anna E. Argento, Phillip E. Kish, Maria G Castro, Pedro R. Lowenstein

Dept. of Cell and Developmental Biology, University of Michigan Medical School, Ann Arbor, 48109 MI, USA
Andrea Comba, Patrick J. Dunn, Daniel B. Zamler, Anna E. Argento, Maria G Castro, Pedro R. Lowenstein

Rogel Cancer Center, University of Michigan medical School, Ann Arbor, 48109, MI, USA

Andrea Comba, Patrick J. Dunn, Daniel B. Zamler, Maria G Castro, Pedro R. Lowenstein

School of Mathematical and Statistical Sciences, Arizona State University, Tempe, AZ, USA
Sebastien Motsch

Ophthalmology & Visual Science, University of Michigan Medical School, Ann Arbor, 48109 MI, USA
Phillip E. Kish, Alon Kahana

Dept. of Pathology, University of Michigan Medical School, Ann Arbor, MI 48109, USA
Celina G. Kleer

Contributions: Conception and design: A. Comba and P. R. Lowenstein. Development of methodology: A. Comba, P. J. Dunn, A. E. Argento, Todd Hollon, D.B. Zamler, P. R. Lowenstein. Acquisition of data, analysis, and interpretation: A. Comba, P. J. Dunn, A. E. Argento, Todd Hollon, D.B. Zamler, M.G. Castro, P. R. Lowenstein. Human histopathology analysis and identification of oncostreams: A. Comba, C. Kleer, A. E. Argento, P. R Lowenstein. Manuscript writing: A. Comba, M. G. Castro, P. R. Lowenstein. Review and/or revision of the manuscript: A. Comba, P. J. Dunn, A. E. Argento, Todd Hollon, D. B. Zamler, C. Kleer, M. G. Castro, P. R. Lowenstein. Administrative, technical, or material support (ie, reporting or organizing data, constructing databases): A. Comba, P. R. Lowenstein. Study supervision: M. G. Castro and P. R. Lowenstein.

Corresponding author:

Correspondence to Pedro R. Lowenstein

ETHICS DECLARATIONS

Competing interests: All authors of this paper declare no potential conflicts of interest.

SUPPLEMENTARY INFORMATION

Supplementary Material and Methods

Supplementary Figures

Supplementary Tables

Fig. 1

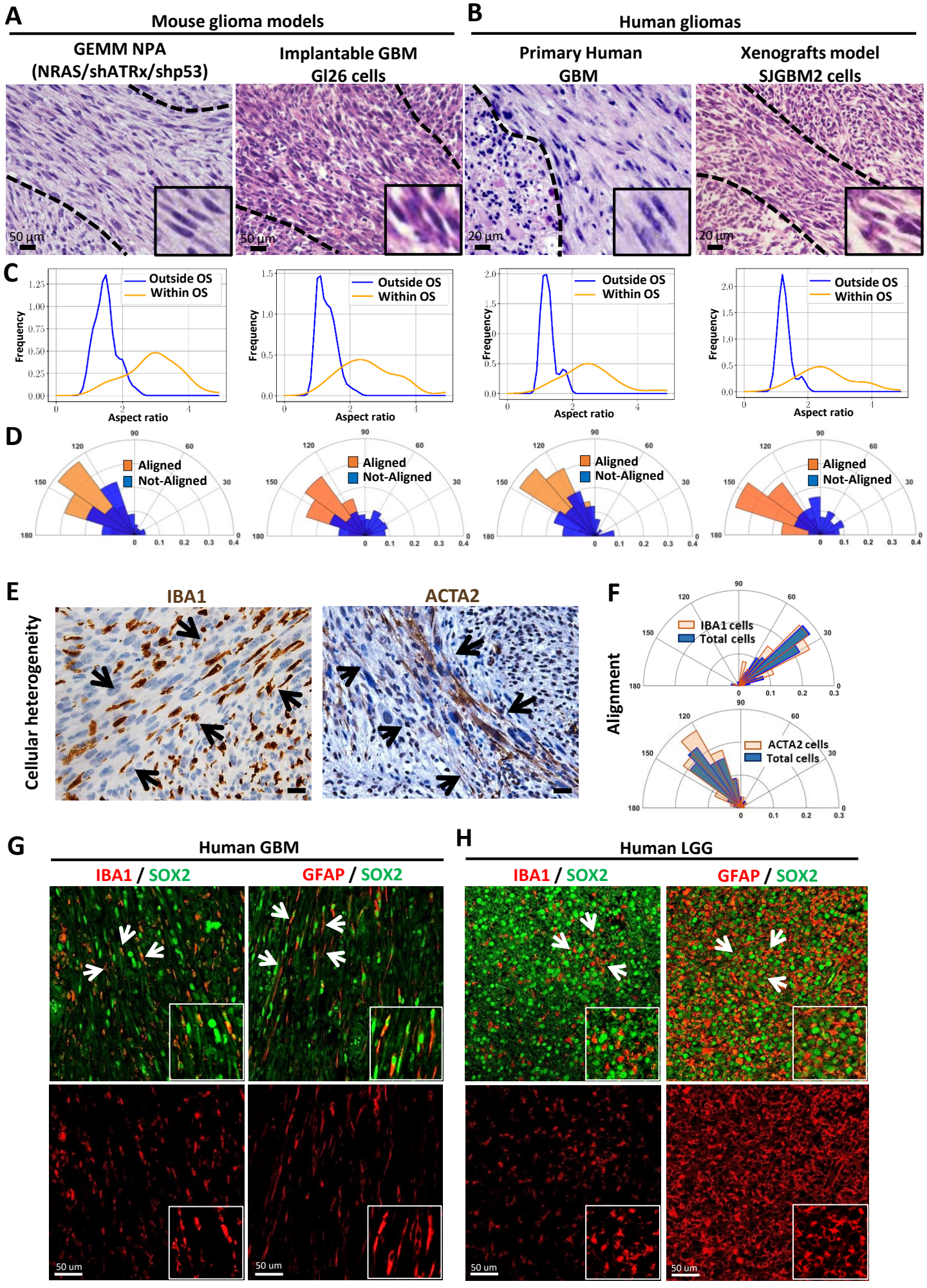
A
Mouse glioma models
GEMM NPA (NRAS/shATRx/shp53)
Implantable GBM Gl26 cells
B
Human gliomas
Primary Human GBM
Xenografts model SJGBM2 cells
50 µm
50 µm
20 µm
20 µm
C
Outside OS
Within OS
Frequency
Aspect ratio
D
Aligned
Not-Aligned
E
IBA1
ACTA2
Cellular heterogeneity
F
Alignment
IBA1 cells
Total cells
ACTA2 cells
Total cells
G
Human GBM
IBA1 / SOX2
GFAP / SOX2
50 um
50 um
H
Human LGG
IBA1 / SOX2
GFAP / SOX2
50 um
50 um

Fig. 1. Oncostreams multicellular fascicles are present in mouse and human gliomas. A) Representative 5 µm H&E microtome sections from gliomas showing that fascicles of spindle-like glioma cells (oncostreams, outlined by the dotted line) are present in a GEMM of gliomas NPA (NRAS/shATRx/shp53) and the GL26 intracranial implantable model of glioma. Scale bars: 50 µm. **B)** Representative H&E microtome sections of human glioma and human xenografts showing the presence of oncostreams. Scale bar: 20 µm. **C-D)** Histograms showing the cellular shape analysis (aspect ratio) (**C**) and angle orientation (alignment) (**D**) shows areas of oncostreams (OS) formed by elongated and aligned cells and areas with no oncostreams (No-OS) as rounded and not-aligned cells. **E-F)** Immunostaining and angle histogram plots show that tumor cells, microglia/macrophages (IBA1+), and mesenchymal cells (ACTA2+), are within, and aligned with, the main orientation axis of oncostreams. Scale bar: 20 µm. **–G-H)** Immuno-fluorescence staining of SOX2+ tumor cells (green), glial fibrillary acidic protein (GFAP+) cells (red), and microglia/macrophage (IBA1+) cells (red) in high-grade human glioblastoma (GBM) (WHO Grade IV), IDH-WT **(G)** and in low-grade glioma (LGG) (WHO Grade III), IDH-mutant **(H)**, showing oncostreams heterogeneity and cellular alignment in human high-grade gliomas. Scale bars: 50 µm.

Fig. 2

A

GEMM of glioma

i)

Tumor	Genetic modifications
NPA	NRAS-GV12/shP53-GFP/shATRX-GFP
NPAI	NRAS-GV12/shP53-GFP/shATRX-GFP/IDH1-R132H

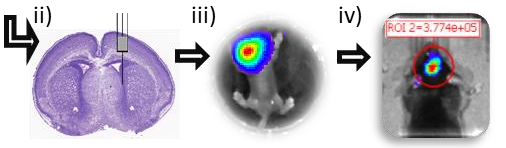

B

Survival analysis

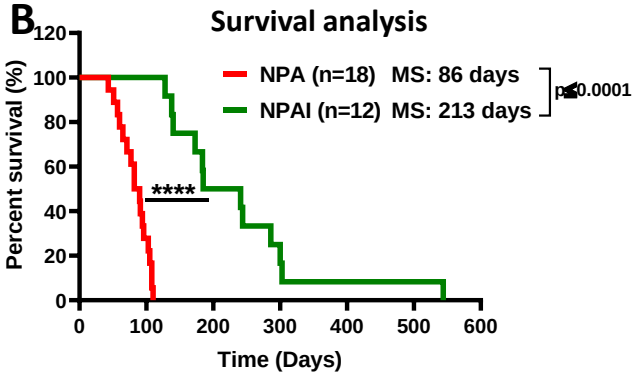

C

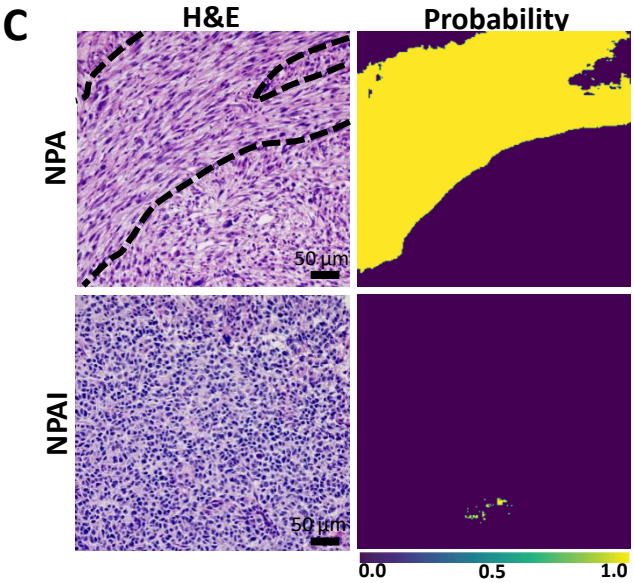

D

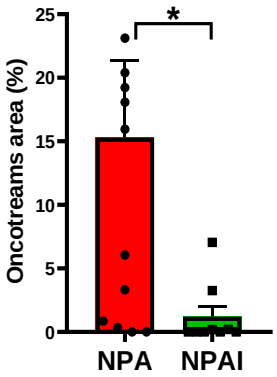

E

Alignment

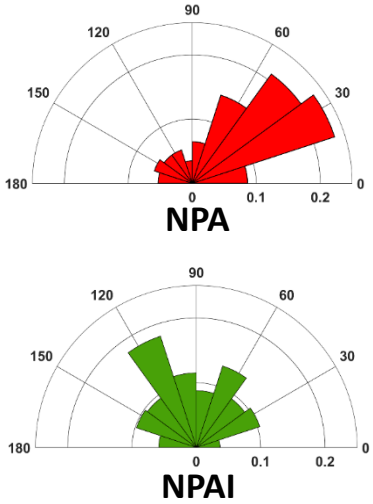

F

Human Gliomas (TCGA)

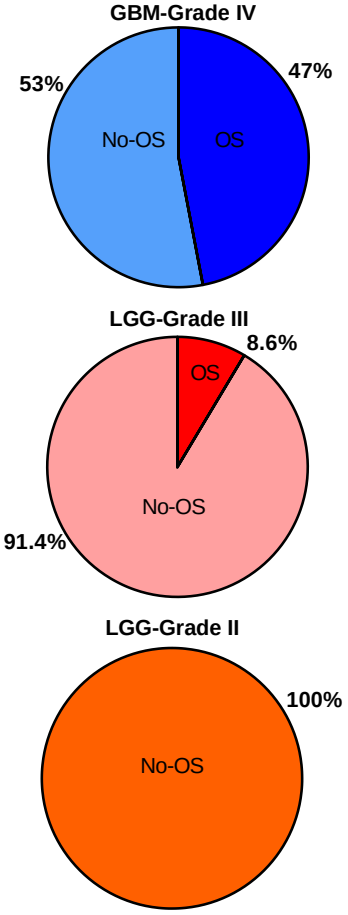

G

H&E

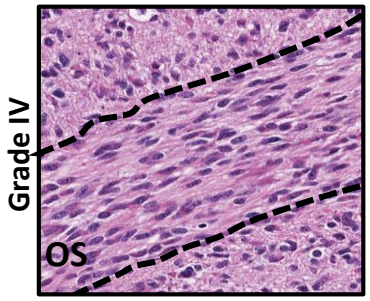

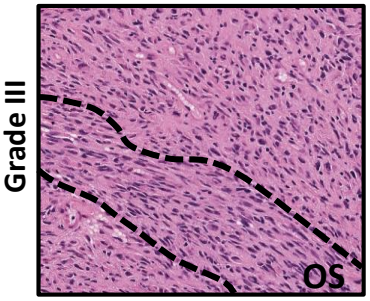

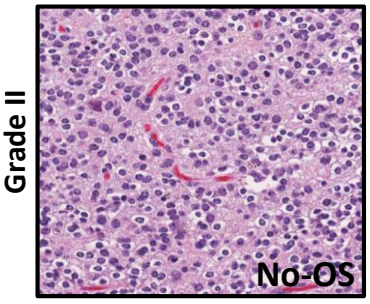

H

Probability heatmap

I

Cell alignment

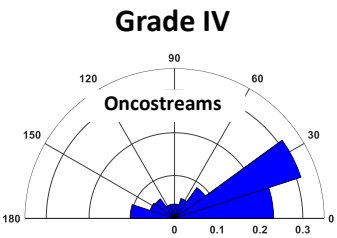

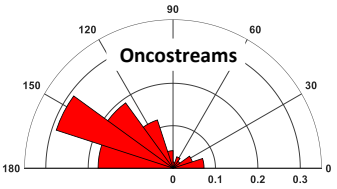

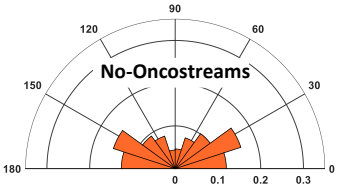

Fig. 2. The density of oncostreams positively correlates with tumor aggressiveness in GEMM of gliomas and human gliomas. A) Schematic representation of the GEMM of glioma generated using the Sleeping Beauty transposase system; i) genetic makeup of NPA and NPAI gliomas, ii) plasmid injection into the lateral ventricle of neonatal mice; iii) bioluminescence imaging of a neonatal mouse 1 day post-injection, iv) bioluminescence detection at 70 days post-injection. **B)** Kaplan–Meier survival curves of NPA and NPAI mouse gliomas show that animals bearing IDH1-R132H mutant tumors (NPAI) have prolonged median survival (MS): **NPA** (MS: 86 days; n: 18) versus **NPAI** (MS: 213 days; n:12). Log-rank (Mantel-Cox) test; ****$p<0.0001$. **C-D)** Deep learning method for oncostream detection on H&E stained mouse glioma sections: **C)** Representative images of oncostreams manually segmented on H&E stained sections of NPA gliomas and NPAI tumors. The output of our trained model for each image is shown below (probability heat maps), for tissues containing oncostreams (NPA), and without oncostreams (NPAI), scale bar = 100 µm. **D)** 10-14 random fields per tumor section per animal were imaged, n=9 NPA and n=12 NPAI, and quantified using deep learning analysis. Error bars represent ± SEM; unpaired t-test analysis, *$p<0.05$. **E)** Angle histogram plots show aligned cells in NPA tumors vs non-aligned cells in NPAI tumors. **F)** Pie charts show percentage of tumors displaying oncostreams in relation to tumor grade. Oncostreams are present in 47% of GBM grade IV tumors, 8.6 % of LGG grade III, and are absent from LGG grade II. **G)** Manual identification of oncostreams in H&E images are shown for human gliomas with WHO grades IV, III, II from TCGA. **H)** Deep learning analysis for human gliomas. Our algorithm was able to detect oncostreams in grade IV and III gliomas but not in grade II gliomas. **I)** Angle histogram plots show the alignment of cells in H&E histology sections of Grade IV and Grade III gliomas' oncostreams and random alignment in grade II glioma sections lacking oncostreams.

Fig. 3

A) Molecular characterization of oncostreams

a) Intracranial GBM

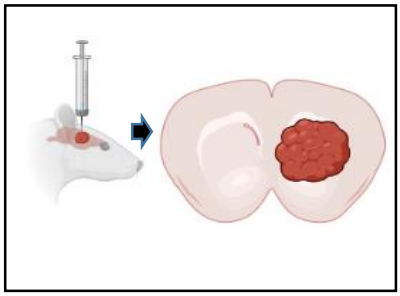

b) Area selection

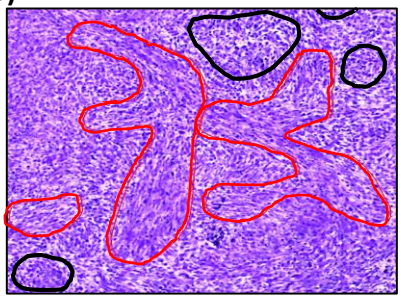

c) LMD dissection

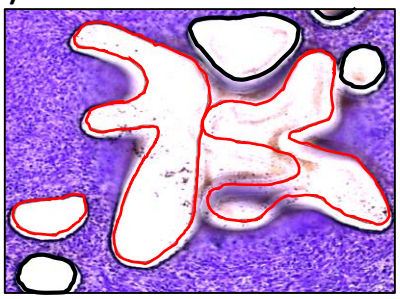

B) Oncostreams *vs* No-Oncostreams

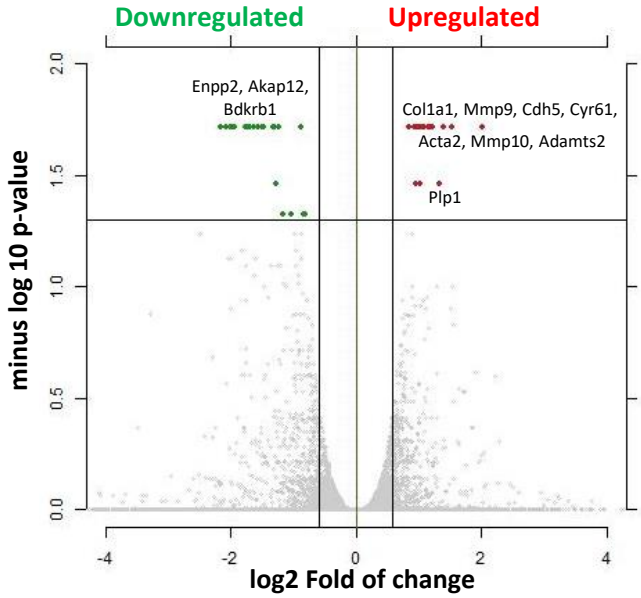

C) DE genes

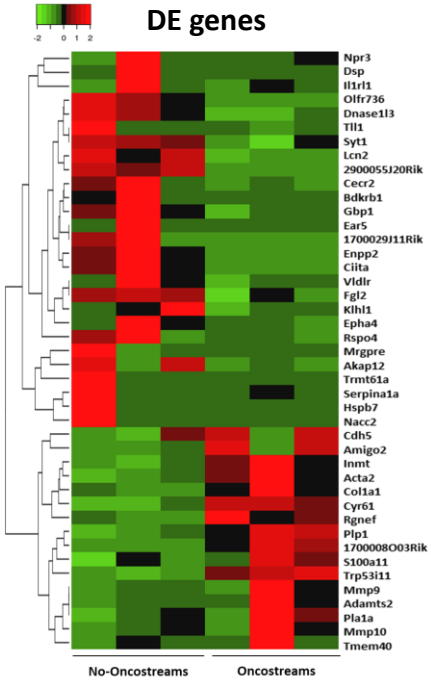

D) GOs Biological processes

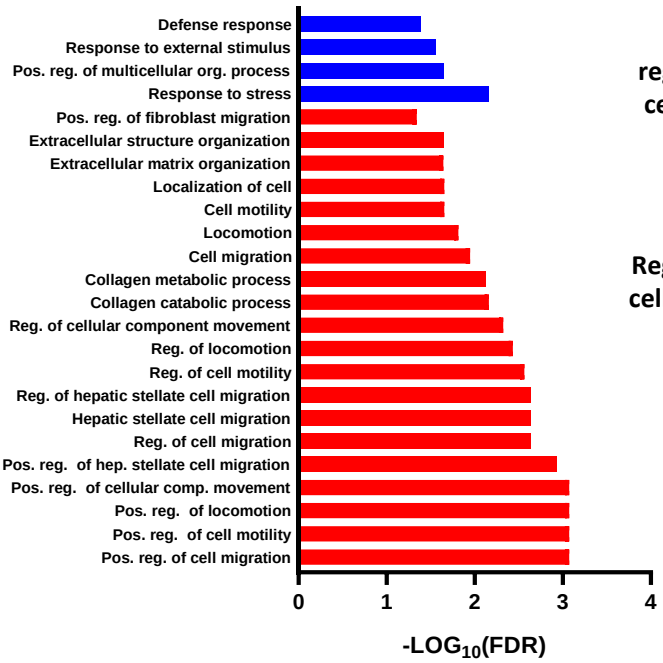

E) DE genes associated to GOs

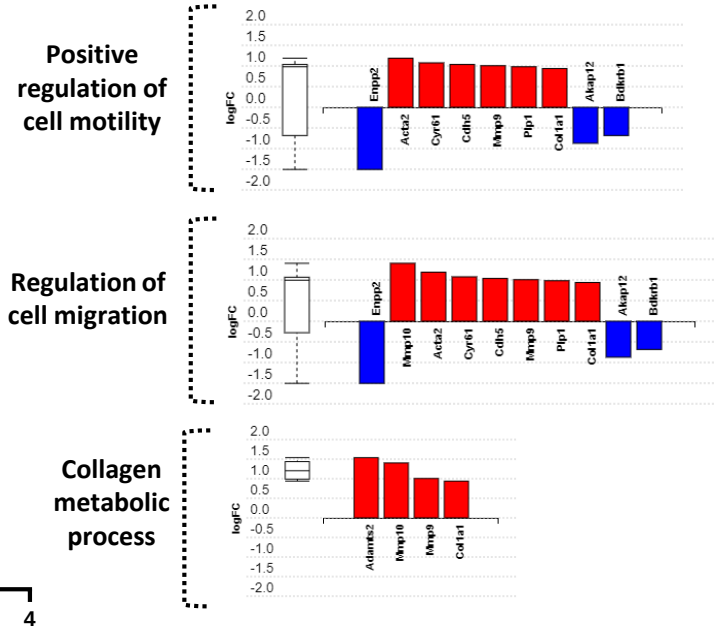

Fig. 3. Oncostreams are defined by a unique gene expression signature related to mesenchymal transformation and migration. A) Schematic representation of spatial transcriptomic analysis of glioma oncostreams using Laser Capture Microdissection (LCM). Glioma tumors were generated by intracranial implantation of NPA tumor cells in C57BL6 mice (a). Oncostream areas (red outline) were identified and dissected from surrounding glioma tissue (black outline) in mouse glioma samples using LCM microscope (b-c). **B)** A volcano plot displays differentially expressed (DE) genes from oncostream *vs* no-oncostream areas. DE genes were selected based on a fold change of ≥ 1.5 and a q-value (false discovery rate (FDR) corrected p-value) of ≤ 0.05. Upregulated genes (red dots) and downregulated genes (green dots) are shown. Relevant genes related to mesenchymal migration–are labeled on the graph. **C)** Heat map illustrates gene expression patterns for oncostream vs no-oncostream areas in NPA glioma tumors (n=3 biological replicates/group). Differentially upregulated genes (n=16) are represented in red and downregulated genes (n=27) are represented in green (q-value ≤ 0.05 and fold change ≥ ± 1.5). **D)** Functional enrichment analysis of overrepresented GO terms (biological processes) obtained when comparing oncostream vs no-oncostream DE genes. p-value corrected for multiple comparisons using the FDR method. Cutoff FDR<0.05. **E)** Bar graphs show DE genes annotated to the most relevant enriched GOs biological process: “Positive regulation of cell motility”, “Regulation of cell migration” and “Collagen metabolic process.”

Fig. 4

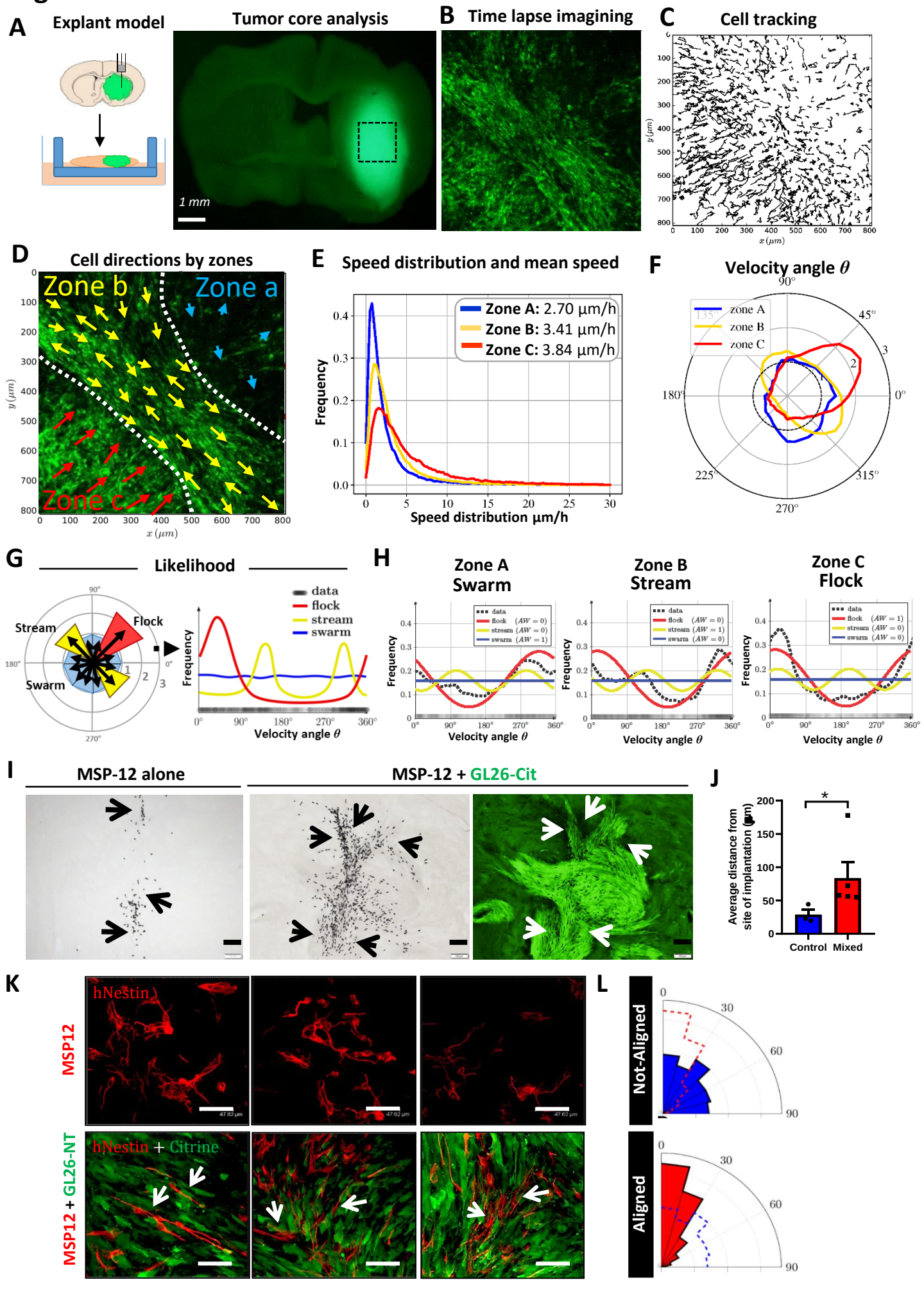
A
Explant model
Tumor core analysis
1 mm
B
Time lapse imagining
C
Cell tracking
D
Cell directions by zones
Zone b
Zone a
Zone c
E
Speed distribution and mean speed
Zone A: 2.70 µm/h
Zone B: 3.41 µm/h
Zone C: 3.84 µm/h
Frequency
Speed distribution µm/h
F
Velocity angle θ
zone A
zone B
zone C
G
Likelihood
Stream
Flock
Swarm
data
flock
stream
swarm
Velocity angle θ
H
Zone A
Swarm
Zone B
Stream
Zone C
Flock
I
MSP-12 alone
MSP-12 + GL26-Cit
J
Average distance from site of implantation (µm)
Control
Mixed
K
MSP12
hNestin
MSP12 + GL26-NT
hNestin + Citrine
L
Not-Aligned
Aligned

Fig. 4. Collective dynamics of oncostreams increase cells' spreading within the tumor core. **A)** Experimental setup: NPA-GFP glioma cells were intracranially implanted in C57BL6 mice. Explant slice cultures were used for confocal time-lapse imaging of the tumor core. **B)** Single representative time-lapse confocal image of glioma cells within the tumor core. **C)** Tracking analysis of individual cell paths performed using the Track-Mate plugin from Image-J. **D)** Preferred direction of cells within three zones (a-c) superimposed onto a representative time lapse-image. **E)** Speed distribution and mean speed ($\mu m/hr$) in Zones A, B and C. **F)** Distribution of velocity angles for each zone. The velocity angle of each cell is denoted ϑ. Plot shows proportion of cells moving in angle direction ϑ for each zone. **G-H)** Classification of collective motion patterns: *stream*, *flock* or *swarm*. The distribution is *uni-modal* for a flock (only one peak) and *bi-model* for a stream (two peaks = 2 preferred velocity angle). For a *swarm*, the distribution is *flat* (no preferred velocity angle). In **(G)** velocity angle was transformed to a histogram; these data were then used to calculate the likelihood that a particular distribution of velocity angles corresponds to either a *stream*, *flock*, or *swarm*. The results are given in **(H)** for each zone. The frequency distribution of the data (shown in black lines) uses a *non-parametric* estimation (kernel density estimator). We tested three types of distributions, ρ, to describe the data-sets and give a likelihood for each case. The best fit was then determined by the Akaike weight (AW). **I)** Co-implantation of highly malignant GL26-citrine cells (green) and human MSP12 glioma stem cells (ratio 1:30), and MSP12 cells alone (control – left image). Immunohistochemistry of human nuclei (black) denote MSP12 cells. Arrows show MSP12 distribution within the brain or the tumor. Scale bar: 100 µm. **J)** Quantification of MSP12 distance from the site of implantation. n=3 for control and n=5 for co-implantation (MSP12+GL26). Error bars ± SEM; t-test analysis, *$p<0.05$. **K)** Immunofluorescence images of human-nestin (red) labeling MSP12 cells, and GL26-citrine cells. Note that MSP12 cells have a multipolar morphological structure when alone, but a bipolar, elongated structure when aligned to GL26-citrine cells. Scale bar: 47.62 µm. **L)** Angle histogram plots quantify the pronounced alignment of MSP12 within oncostreams, and random alignment of MSP12 cells when implanted alone (with dashed overlays of the other condition's alignment).

Fig. 5

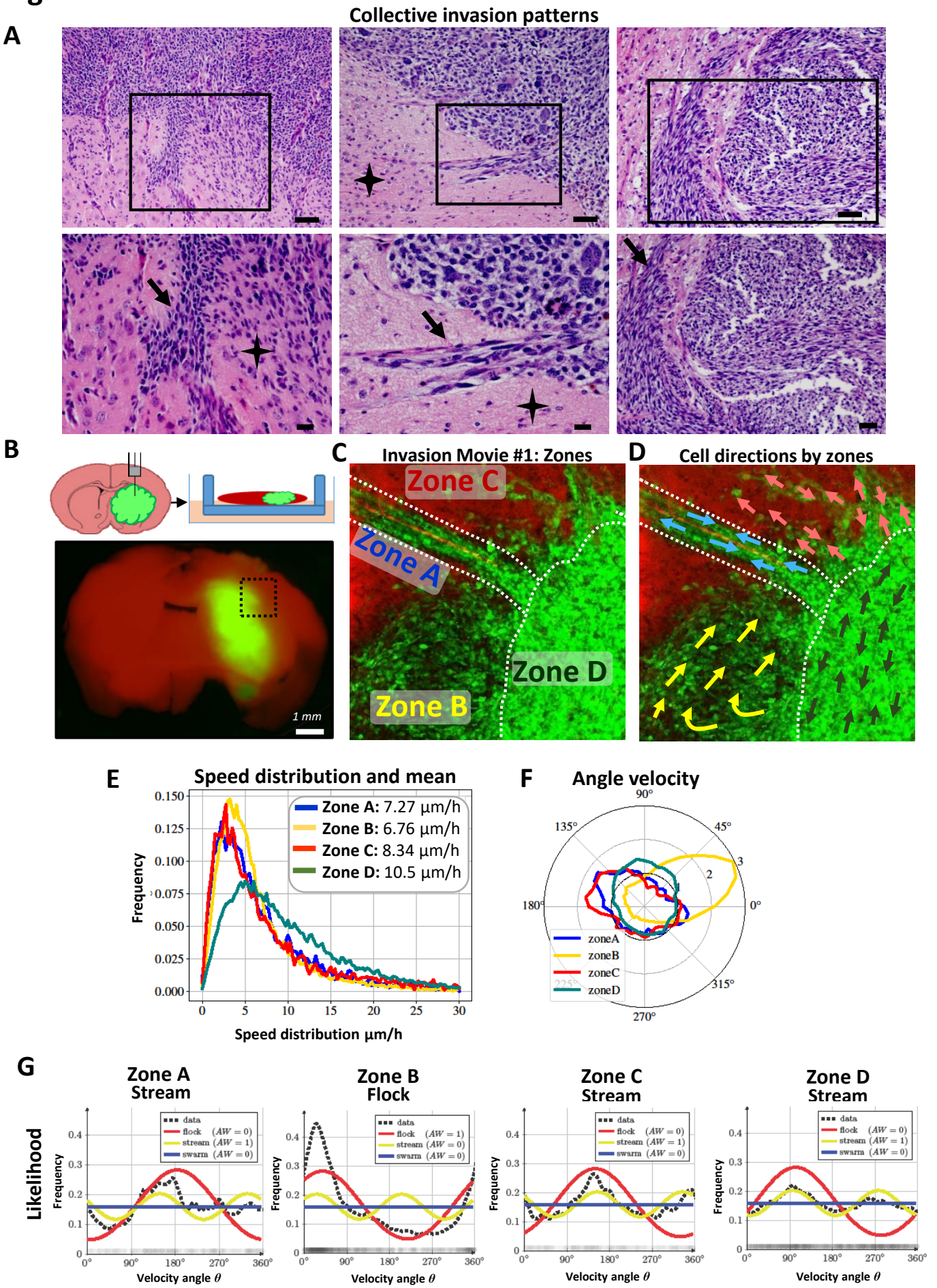
Collective invasion patterns
A
B
1 mm
C
Invasion Movie #1: Zones
Zone C
Zone A
Zone D
Zone B
D
Cell directions by zones
E
Speed distribution and mean
Zone A: 7.27 µm/h
Zone B: 6.76 µm/h
Zone C: 8.34 µm/h
Zone D: 10.5 µm/h
Frequency
Speed distribution µm/h
F
Angle velocity
90°
45°
135°
180°
0°
225°
315°
270°
zoneA
zoneB
zoneC
zoneD
G
Likelihood
Zone A Stream
Zone B Flock
Zone C Stream
Zone D Stream
data
flock (AW = 0)
stream (AW = 1)
swarm (AW = 0)
Frequency
Velocity angle θ

Fig. 5. Collective invasion of oncostreams contributes to malignant glioma behavior. A) Representative images of oncostream invasion (top row, black boxes) from H&E stained sections of GEMM of glioma. Arrows indicate oncostream collective invasion. Areas highlighted by black boxes are shown at higher magnification in the lower row. Stars indicate sites of single cell invasion. Scale bars: 50 µm (top) and 20 µm (bottom). **B)** Schematic representation of the experimental setup and location of imaging of tumor borders using td/mtTomato mice. **C)** Representative time-lapse scanning confocal image of glioma cells at the tumor border. This image was taken from border movie #1. Differentiation of dynamics zones. **D)** Preferred direction of cells within different zones superimposed onto a representative time lapse-image. **E)** Histogram of speed distribution and mean speed ($\mu m/h$) of Zones A, B, C and D. **F)** Velocity angle distribution analysis (ϑ) performed by zones. Plot shows overall direction and magnitude of cell movement. **G)** Likelihood analysis of the dynamic patterns at the tumor border. Graph of density estimation *ρ flock* (red), *ρ stream* (yellow) and *ρ swarm* (blue). The estimation of the black line uses a *non-parametric* estimation. AW: 0 or AW:1.

Fig. 6

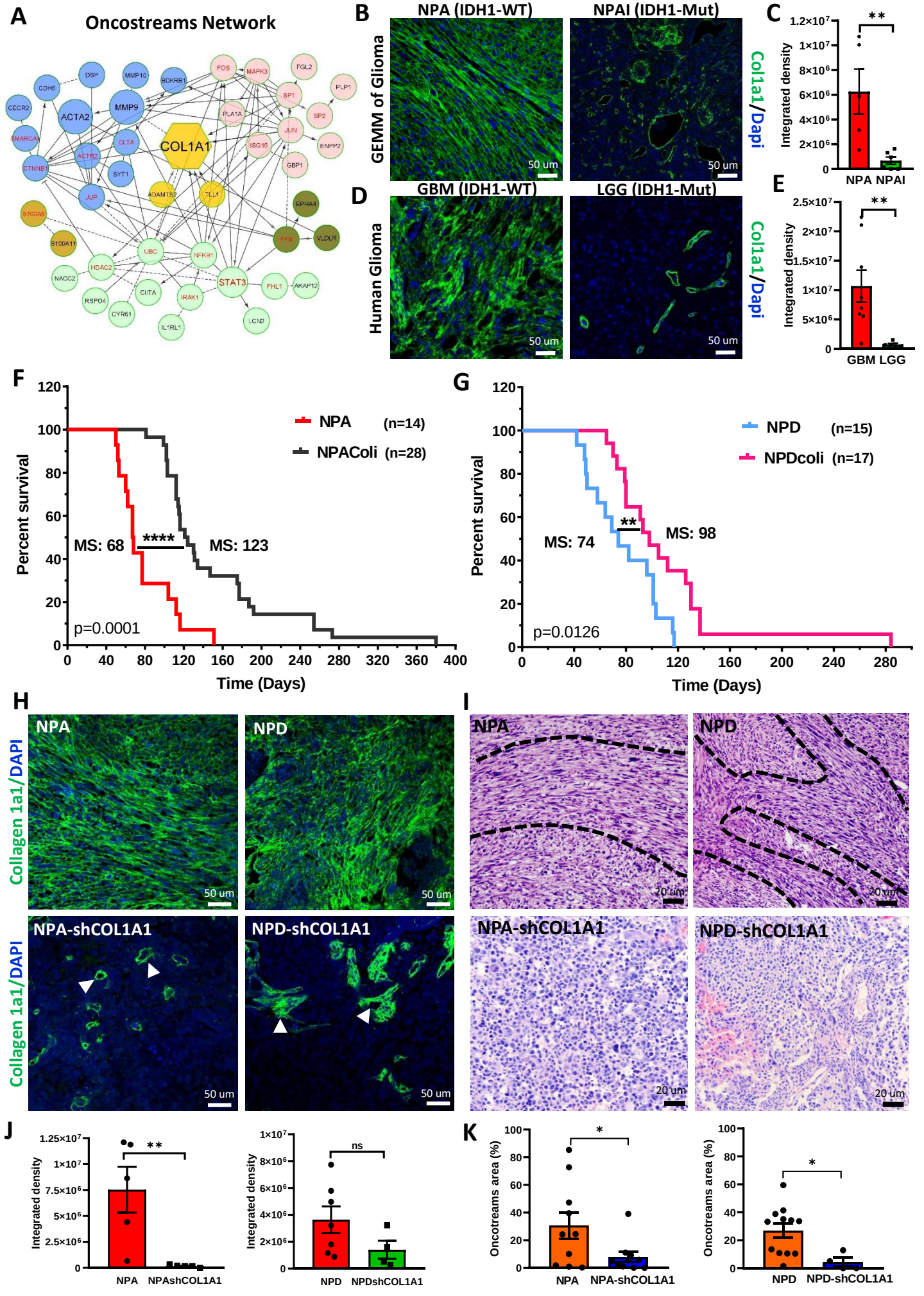
A
Oncostreams Network
COL1A1
ACTA2
MMP9
B
NPA (IDH1-WT)
NPAI (IDH1-Mut)
GEMM of Glioma
Col1a1/Dapi
50 um
C
Integrated density
NPA NPAI
D
GBM (IDH1-WT)
LGG (IDH1-Mut)
Human Glioma
E
GBM LGG
F
NPA (n=14)
NPAColi (n=28)
MS: 68
MS: 123
****
p=0.0001
Percent survival
Time (Days)
G
NPD (n=15)
NPDcoli (n=17)
MS: 74
MS: 98
**
p=0.0126
H
Collagen 1a1/DAPI
NPA
NPD
NPA-shCOL1A1
NPD-shCOL1A1
I
20 um
J
NPA NPAshCOL1A1
NPD NPDshCOL1A1
ns
K
Oncotreams area (%)
NPA-shCOL1A1
NPD-shCOL1A1

Fig. 6. Col1a1 is a central hub in oncostream organization and glioma malignancy. A) Network analysis of the DE genes comparing oncostreams versus no-oncostreams DE genes. Genes with a higher degree of connectivity are highlighted with larger nodes. Clusters of nodes with the same color illustrate modules of highly interacting of genes in the network. **B)** Immunofluorescence analysis of COL1A1 expression in GEMM of glioma tissues comparing NPA (IDH1-WT) vs NPAI (IDH1mut). Representative confocal images display COL1A1 expression in green (Alexa 488) and nuclei in blue (DAPI). Scale bar: 50 µm. **C)** Bar graphs represent COL1A1 quantification in terms of fluorescence integrated density. n= 5-6 animals for each experimental condition were used for the analysis. Ten fields of each tumor section were selected at random. Error bars represent ±SEM. t-test, **p<0.01. **D)** Immunofluorescence analysis of COL1A1 expression in human GBM and LGG tumors. COL1A1 expression in green (Alexa 488) and nuclei in blue (DAPI). Scale bar: 50 µm. **E)** Bar graphs represent COL1A1 quantification as fluorescence integrated density. 5 (LGG) and 8 (GBM) tumor samples were used for the analysis. Ten fields of each tumor section were selected at random. Error bars represent ±SEM. t-test, **p<0.01. **F-G)** GEMM of glioma with COL1A1 inhibition. **F)** Kaplan–Meier survival curve comparing NPA (MS: 68 days; n: 14) vs NPAshCOL1A1 (MS: 123 days; n: 28) **G)** Kaplan–Meier survival curve comparing NPD (MS: 74 days; n=15) versus NPDshCOL1A1 (MS: 98 days; n=17). Log-rank (Mantel-Cox) test. **** p<0.0001, **p<0.0126. **H)** Immunofluorescence analysis of COL1A1 expression in GEMM of glioma controls (NPA and NPD) and GEMM of gliomas with Col1A1 downregulation (NPAshCOL1A1 and NPDshCOL1A1). Representative confocal images of COL1A1 expression in green (Alexa 488) and nuclei in blue (DAPI). Scale bar: 50 µm. **J)** Bar graphs represent COL1A1 quantification in terms of fluorescence integrated density. 5-7 tumor samples for each experimental condition were used for the analysis. Ten fields of each tumor section were selected at random. Error bars represent ±SEM. t-test, **p<0.01. **I)** Representative images of the histopathological identification of in H&E tissue sections comparing the COL1A1 knockdown tumors with their respective controls. Magnification: 20x. Scale bars: 50 µm. **K)** Quantitative analysis of oncostream areas using deep learning analysis. 4-12 tumor samples for each experimental condition were used for the analysis. Error bars represent ± SEM; unpaired t-test analysis, *p<0.05.

Fig. 7

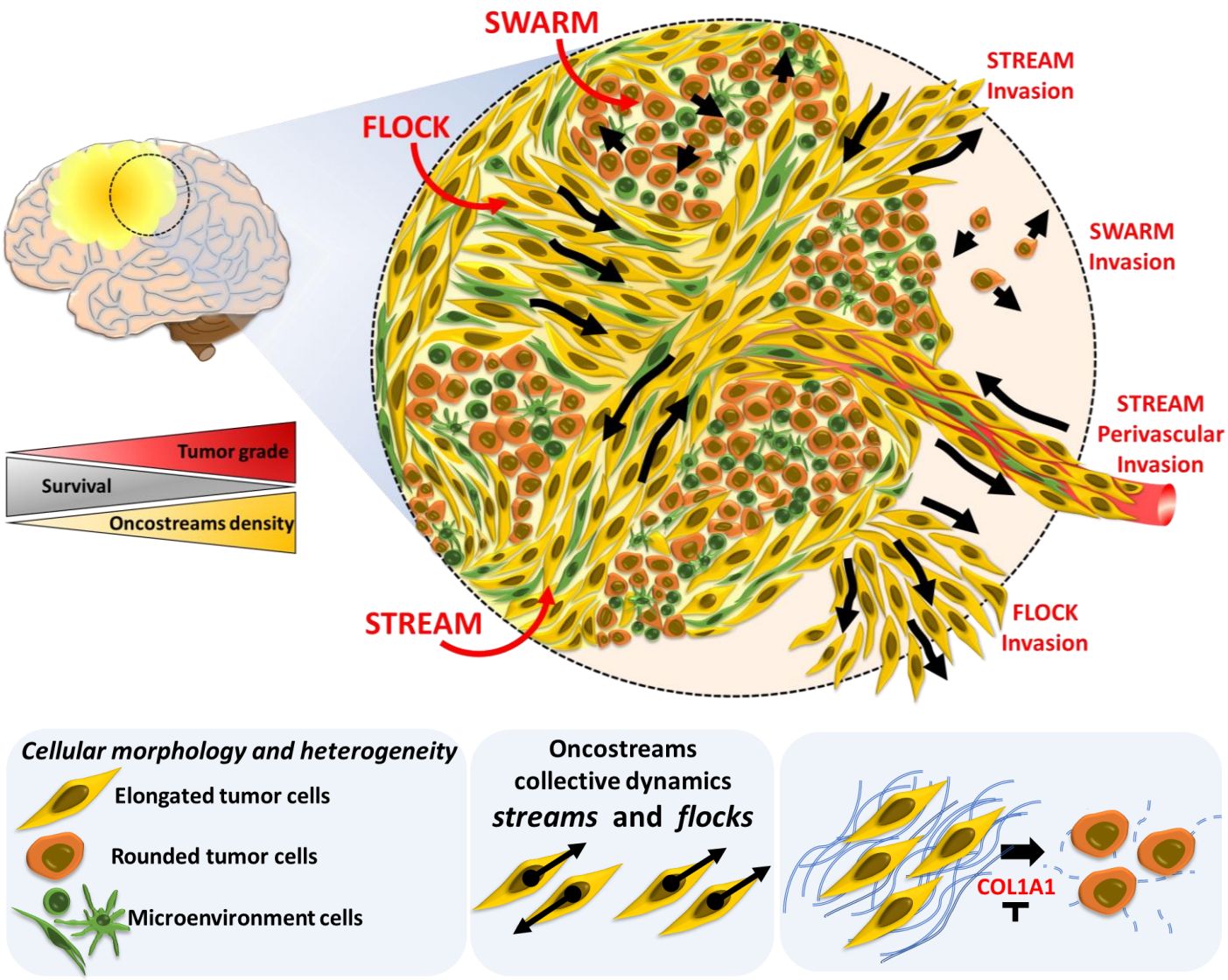

Fig. 7. Oncostreams are COL1A1-rich multicellular dynamic mesenchymal structures that regulate glioma invasion and malignancy. Summary representation of mesenchymal dynamic fascicles (oncostreams) present in high grade gliomas. Our study reveals that oncostreams display directional collective motility patterns including streams and flocks. Non-directional collective motion (swarms) are represented by round cells that move randomly. Directional dynamic patterns function as tumoral highways to facilitate the intra-tumoral spread of cells and participate in local invasion of normal brain. Oncostreams are areas of mesenchymal transformation defined by a molecular signature enriched in COL1A1. COL1A1 knockdown disrupts oncostream organization, decreases intratumoral heterogeneity and significantly increases animal survival. Our study reveals that oncostreams are anatomically and molecularly distinctive, are areas of mesenchymal transformation organized through interactions with the COL1A1 matrix, move by collective motion, and regulate glioma growth and invasion.